AGU PUBLICATIONS

Global Biogeochemical Cycles

RESEARCH ARTICLE
10.1002/2014GB004920

This article is a companion to *Grand et al.* [2015] doi:10.1002/2014GB004898.

Key Points:
- Upper 1000 m dissolved Fe and Al CLIVAR section from Antarctica to Bay of Bengal
- Interaction of ACC with Kerguelen Plateau may produce elevated subsurface Fe
- High Fe >100 m in north Indian Ocean from remineralization and shelf inputs

Supporting Information:
- Readme
- Figure S1
- Figure S2
- Figure S3

Correspondence to:
M. M. Grand,
maxime@hawaii.edu

Citation:
Grand, M. M., C. I. Measures, M. Hatta, W. T. Hiscock, W. M. Landing, P. L. Morton, C. S. Buck, P. M. Barrett, and J. A. Resing (2015), Dissolved Fe and Al in the upper 1000 m of the eastern Indian Ocean: A high-resolution transect along 95°E from the Antarctic margin to the Bay of Bengal, *Global Biogeochem. Cycles*, *29*, 375–396, doi:10.1002/2014GB004920.

Received 22 JUN 2014
Accepted 16 FEB 2015
Accepted article online 17 FEB 2015
Published online 31 MAR 2015

Dissolved Fe and Al in the upper 1000 m of the eastern Indian Ocean: A high-resolution transect along 95°E from the Antarctic margin to the Bay of Bengal

Maxime M. Grand[1], Christopher I. Measures[1], Mariko Hatta[1], William T. Hiscock[2], William M. Landing[3], Peter L. Morton[3], Clifton S. Buck[4], Pamela M. Barrett[5], and Joseph A. Resing[5]

[1]Department of Oceanography, University of Hawaii, Honolulu, Hawaii, USA, [2]Thermo Fisher Scientific, North Ryde, New South Wales, Australia, [3]Department of Earth, Ocean and Atmospheric Science, Florida State University, Tallahassee, Florida, USA, [4]Skidaway Institute of Oceanography, University of Georgia, Savannah, Georgia, USA, [5]Joint Institute for the Study of the Atmosphere and Ocean, University of Washington and PMEL/NOAA, Seattle, Washington, USA

Abstract A high-resolution section of dissolved iron (dFe) and aluminum (dAl) was obtained along ~95°E in the upper 1000 m of the eastern Indian Ocean from the Antarctic margin (66°S) to the Bay of Bengal (18°N) during the U.S. Climate Variability and Predictability (CLIVAR) CO_2 Repeat Hydrography I08S and I09N sections (February–April 2007). In the Southern Ocean, low concentrations of dAl (<1 n*M*) reflect the negligible dust inputs impacting the water masses subducted in the circumpolar domain. The low dAl concentrations characterizing the Southern Ocean terminate near 45°S, probably because of the advection of subtropical water masses that received dust and sedimentary inputs in their formation region. Our subsurface dFe data near the southern Kerguelen Plateau were significantly higher than historical observations in other Indian sectors of the Southern Ocean. We surmise that the offshore advection of dFe-rich waters along the western flank of the southern Kerguelen plateau and enhanced vertical mixing could contribute to this elevated subsurface dFe inventory. Elevated subsurface particulate and dFe levels downstream of the northern Kerguelen Plateau may reflect long-range lateral transport from the plateau's sediments and/or remineralization inputs. At the northern edge of the south Indian subtropical gyre, the deposition of Australian dust, possibly combined with the advection of dAl-enriched waters from the Indonesian Throughflow, creates a region of elevated dAl in the upper 400 m but without a corresponding enrichment in dFe. In the northern Indian Ocean, the South Equatorial Current constitutes a remarkable biogeochemical front separating the oxygen-rich and dFe-poor subtropical gyre waters from the dFe-rich and oxygen-depleted waters of the northern Indian Ocean. By tracing the accumulation of macronutrients and dFe along the advective pathway of Indian Central Water, we show that the central waters of the northern Indian Ocean receive excess dFe in addition to that produced by remineralization inputs. The resuspension of shelf sediments and release of pore waters probably contribute to the elevated dFe and dAl levels observed below the highly stratified upper layers of the Bay of Bengal.

1. Introduction

The availability of iron (Fe) relative to the supply of macronutrients in vast regions of the oceans influences marine productivity and may contribute to the regulation of atmospheric CO_2 levels over glacial-interglacial timescales [*Martin*, 1990; *Martínez-Garcia et al.,* 2009, 2014]. For this reason, there has been a strong motivation to incorporate parameterizations of the Fe cycle into global ocean biogeochemical models of varying complexity [*Archer and Johnson*, 2000; *Aumont et al.*, 2003; *Parekh et al.,* 2004, 2005; *Moore and Braucher*, 2008; *Misumi et al.,* 2013; *Tagliabue et al.,* 2014a]. Although ocean general circulation and biogeochemistry models will ultimately provide the best means to assess the relative contribution of various Fe sources to the contemporary oceanic Fe cycle and to test its sensitivity to anthropogenic forcing, the development of a global database of Fe observations is first required to constrain simulations and, if needed, improve model parameterizations [*SCOR Working Group*, 2007]. Over the last three decades, the database of Fe observations has been greatly expanded during localized sampling campaigns and, more recently, through basin-scale transects as part of the Climate Variability and Predictability (CLIVAR) [*Grand et al.,* 2014] and GEOTRACES [*Anderson et al.,* 2014] programs [*Measures et al.,* 2008a; *Middag et al.,* 2009, 2011; *Klunder et al.,* 2011,

2012; *Hatta et al.,* 2014; *Rijkenberg et al.,* 2014]. However, vast areas of the oceans still remain where the density of observations is inadequate or completely absent.

Sampling for trace elements along selected sections of the U.S. CLIVAR CO_2 Repeat Hydrography Program has provided an unprecedented opportunity to produce high-resolution sections of dissolved Fe and aluminum (Al) in the upper 1000 m of the Atlantic, Pacific, and Indian Oceans [*Measures et al.,* 2008a; *Grand et al.,* 2014]. The principal motivations for measuring dissolved Fe and Al simultaneously on these sections relate to the importance of dust deposition in delivering Fe to the remote ocean [*Jickells et al.,* 2005] and the utility of dissolved Al as a tracer of dust deposition inputs to the remote surface ocean, because Al has no known biological requirement and has a longer residence time than Fe in the upper ocean [*Measures and Brown*, 1996; *Measures and Vink*, 2000]. Below the surface, the distribution of dissolved Al can be impacted by long-range transport of water masses that have been labeled with Al by dust deposition in their ventilation region [*Measures et al.,* 2008a], or from the resuspension of sediments and release of pore waters near continental margins [*Hatta et al.,* 2013; *Middag et al.,* 2012, 2013].

The Indian Ocean is one of the most undersampled and least understood basin of the world oceans in terms of its physical and biogeochemical dynamics [*Hood et al.,* 2009]. The dearth of observations in the Indian Ocean is particularly striking for Fe and Al, which have been sampled at only a handful of locations west of Ninety East Ridge [*Nishioka et al.*, 2013; *Vu and Sohrin*, 2013] and in the Arabian Sea [*Saager et al.*, 1989; *Measures and Vink*, 1999; *Moffett et al.*, 2007; *Kondo and Moffett*, 2013]. Our current knowledge of the distributions of dissolved Fe and Al is even more limited in the eastern Indian Ocean, where previous observations consist of six soluble ($<$0.04 μm) Al profiles from 40°S to 10°N along 90°E–110°E [*Obata et al.,* 2004] and one full-depth vertical profile of dissolved Al and Fe in the Bay of Bengal [*Vu and Sohrin*, 2013]. In contrast, the Southern Ocean sector of the Indian Ocean has received more attention, with repeated observations in the naturally Fe-fertilized waters of the Kerguelen and Crozet plateaus [*Sarthou et al.*, 1997; *van Beusekom et al.*, 1997; *Bucciarelli et al.*, 2001; *Planquette et al.*, 2007; *Blain et al.*, 2008] and south of Australia and Tasmania [*Sohrin et al.,* 2000; *Sedwick et al.*, 2008; *Bowie et al.*, 2009].

This work is concerned with a high-resolution meridional section of dissolved ($<$0.4 μm) Fe and Al in the upper 1000 m of the eastern Indian Ocean obtained during the U.S. CLIVAR CO_2 I08S and I09N Repeat Hydrography sections (Figure 1). This paper identifies the dominant source terms for each element from the Antarctic margin to the Bay of Bengal in the context of the known physical and biogeochemical dynamics of the eastern Indian Ocean. A companion paper describes the surface distribution of Al and Fe of this section in more detail, with a particular focus on the biogeochemical impacts of dust deposition in the surface layer [*Grand et al.*, 2015]. The data presented here allow the investigation of Fe and Al cycling across a wide range of biogeochemical regimes and atmospheric deposition gradients. In particular, the Southern Ocean sector considered in this work is located in the vicinity of the Kerguelen Plateau, which is characterized by negligible dust inputs and anomalously elevated productivity. The south Indian subtropical gyre is impacted by dust emanating from Australia and, at its northern edge, by the outflow of waters of Indonesian origin carried by the South Equatorial Current (SEC). The northern end of the section allows investigation of the biogeochemistry of Fe and Al across a remarkable biogeochemical gradient from the SEC to the Bay of Bengal. The latter is characterized by oxygen-deficient waters beneath a highly stratified surface layer, the largest dust fluxes of the transect and enormous riverine inputs of freshwater and suspended sediments from the Ganges-Brahmaputra and peninsular rivers discharging into the Bay of Bengal. The present data set is the first of its kind for the eastern Indian Ocean and will provide valuable constraints on numerical model simulations of Fe and Al in the Indian Ocean.

2. Materials and Methods

2.1. Sample Collection and Shipboard Analysis

Seawater samples were collected aboard the R/V *Roger Revelle* during the U.S. CLIVAR CO_2 Repeat Hydrography I08S and I09N cruises following the trace metal clean protocols of *Measures et al.* [2008b]. The I08S transect was started in the Indian sector of the Southern Ocean at the edge of the Antarctic margin (65.8°S) in late austral summer (15 February 2007) and was completed in the central south Indian subtropical gyre (28.3°S) on 13 March 2007. Sampling resumed on the I09N transect on 27 March starting from the last station of I08S and ending a month later (27 April 2007) at 18°N in the Bay of Bengal (hereinafter referred to as BoB). The data set

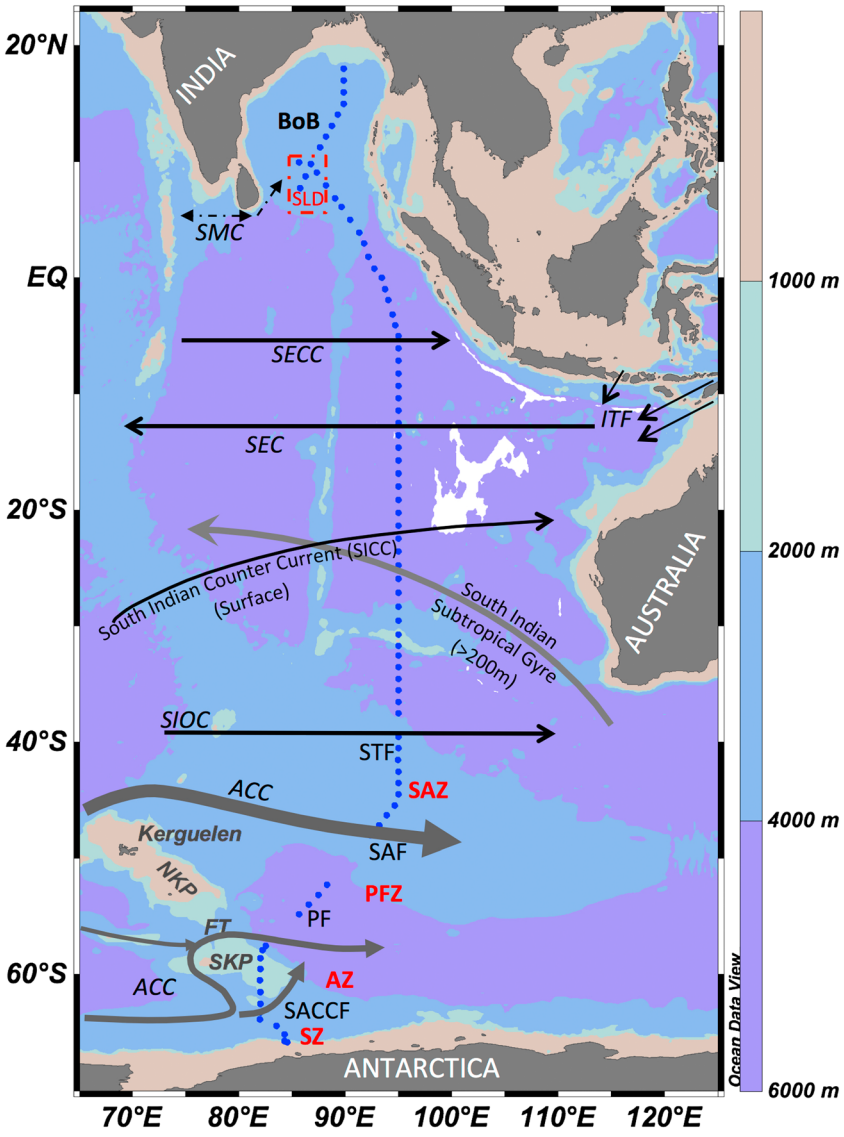

Figure 1. Cruise track, fronts, and principal currents along the CLIVAR I08S & I09N sections. Blue dots show the 85 trace metal stations sampled. The color bar legend refers to the bathymetry. ACC: Antarctic Circumpolar Current; SKP: Southern Kerguelen Plateau; FT: Fawn Trough; NKP: Northern Kerguelen Plateau; SACCF: South ACC Front; PF: Polar Front; SAF: Sub-Antarctic Front; STF: Subtropical Front; SZ: Southern Zone; AZ: Antarctic Zone; PFZ: Polar Frontal Zone; SAZ: Subantarctic Zone; SIOC: South Indian Ocean Current; SEC: South Equatorial Current; ITF: Indonesian Throughflow; SECC: South Equatorial Counter Current; SMC: Southwest Monsoon Current; BoB: Bay of Bengal; SLD: Sri Lanka dome. Double headed arrows denote seasonally reversing (monsoonal) currents. The red dashed rectangle shows the seasonally productive region of the Sri Lanka dome (SLD).

encompasses a total of eighty-five 12-depth vertical profiles spaced at approximately 1° intervals in the upper 1000 m of the eastern Indian Ocean along 82°E–95°E (Figure 1). There are gaps in the coverage near 55°S and 50°S in the Southern Ocean, because rough seas prevented deployment of the trace metal rosette from the stern of the ship.

Upon recovery of the rosette, seawater samples were filtered in a clean van through 0.4 μm acid washed 47 mm polycarbonate (GE-Poretics K04CP04700) track-etched membrane filters [*Measures et al.,* 2008b]. The filtrates were stored in the dark in an airconditioned laboratory container at ~25°C in 125 mL acid-cleaned polymethylpentene (PMP) bottles until shipboard analysis, which was usually performed within 48 h of collection. Prior to analysis, the filtered samples were acidified with 125 μL of 6 *M* HCl, which was purified by

sub-boiling point distillation in a quartz glass still. The PMP bottles containing the acidified samples (pH = 2.2) were then heated to 60 ± 10°C in a 900 W microwave oven and allowed to cool to ambient temperature for about 1 h. Analysis of dissolved Fe and Al (hereinafter referred to as dFe and dAl, respectively) was performed in groups of 24–36 samples using the flow injection analysis (FIA) protocols of *Measures et al.* [1995] and *Resing and Measures* [1994], respectively. The FIA manifold was calibrated at regular intervals using filtered seawater of low dFe and dAl content prepared in the same way as the samples and spiked with commercial Fe and Al standards. The PMP bottles containing the stock standards were stored in a refrigerator at 4°C within a double plastic bag to prevent evaporation. The detection limits, defined as 3 times the standard deviation of replicate 2.5 mL loads ($n = 16$) of a Southern Ocean surface sample, were 0.07 n*M* for dFe and 0.30 n*M* for dAl.

The FIA system dFe blank was estimated by spiking an acidified seawater sample (pH = 2.2) with 80 μ*M* ethylenediaminetetraacetic acid (EDTA) and analyzing it along with unspiked samples during an analytical run day. The resulting signal was then subtracted from all raw dFe values produced on that day. No detectable acid or sample buffer blank was identified with the Al system. When necessary, the dFe and dAl data were drift corrected using the slopes of the calibration curves to compensate for variations in instrumental sensitivity during the course of a day.

2.2. Data Quality Control and Data Repository

Data quality flags were assigned to dFe and dAl data following the World Ocean Circulation Experiment (WOCE) flag convention. A linear regression between the conductivity-temperature-depth (CTD) salinity and that measured on discrete water samples was used to identify GO-FLO sampling bottles that did not close at the specified depth. These samples were excluded from further analyses. Outliers observed on individual dFe and dAl vertical profiles were carefully examined before assigning a quality flag. If the magnitude of the observed anomaly was inconsistent with data from adjacent stations and/or other hydrographic parameters (salinity, θ, N, P, and Si), then the sample was excluded due to suspected contamination. The EDTA blank correction for dFe was exceptionally high for 13 consecutive stations between 41.5°S and 28.3°S and applying the correction yielded slightly negative surface dFe values at some stations in this latitudinal band. Typically, the magnitude of the FIA system blank for dFe is verified postcruise by comparing a subset of each day's shipboard run against data obtained by inductively coupled plasma–mass spectrometry (ICP-MS) analysis on replicate stored samples [*Measures et al.,* 2008b]. Unfortunately, it was only possible to compare our dFe data with those of ICP-MS at four stations in the Bay of Bengal, because the remaining stored sample bottles appeared to be contaminated with dFe. Since we are unsure of the validity of this part of the data set, we conservatively excluded the dFe data from 41.5°S to 28.3°S. Overall, 4% and 18% of the analyzed dAl and dFe samples were eliminated, respectively.

The SAFe reference standards were not analyzed during this cruise because the pH of that standard is incompatible with our shipboard methodology, which was originally designed to handle samples acidified with 1 mL 6 M HCl/L, not the 4 mL 6 M HCL/L of the SAFe standards. Nevertheless, we were able to compare our shipboard dFe values with those run via ICP-MS at four stations in the Bay of Bengal, where the stored replicate samples did not appear to be compromised. At the four stations in the Bay of Bengal, an ordinary least squares fit between the shipboard and ICP-MS dFe data sets suggests that there is no apparent offset between the two methods (slope ± SE = 1.01 ± 0.06; intercept ± SE: −0.05 ± 0.06; $R^2 = 0.90$, $n = 33$). The accuracy of the ICP-MS determinations at these four stations was assessed by analyzing the SAFe reference samples. The dFe values measured by ICP-MS in the SAFe-S and SAFe-D2 samples were 0.099 ± 0.054 n*M* ($n = 3$) and 0.890 ± 0.09 n*M* ($n = 3$), respectively, and compare well with the consensus values (SAFe-S: 0.093 ± 0.008 n*M*; SAFe-D2: 0.933 ± 0.023 n*M*).

All dFe and dAl data and ancillary parameters (e.g., Lowered Acoustic Doppler Current Profiler (LADCP) velocities and dissolved inorganic carbon (DIC)) used in this paper are publicly available on the CLIVAR & Carbon Hydrographic Data Office website (CCHDO) using ExpoCodes 33RR20070204 and 33RR20070322 for I08S and I09N, respectively (http://cchdo.ucsd.edu). Note that particulate metal concentrations in total suspended matter collected on the 0.4 μm acid washed 47 mm polycarbonate filters were analyzed by energy-dispersive X-ray fluorescence as described in *Barrett et al.* [2012]. Although these data will be published elsewhere, we refer to a subset of this data set in the interpretation of our dFe and dAl data in the Southern Ocean and Bay of Bengal.

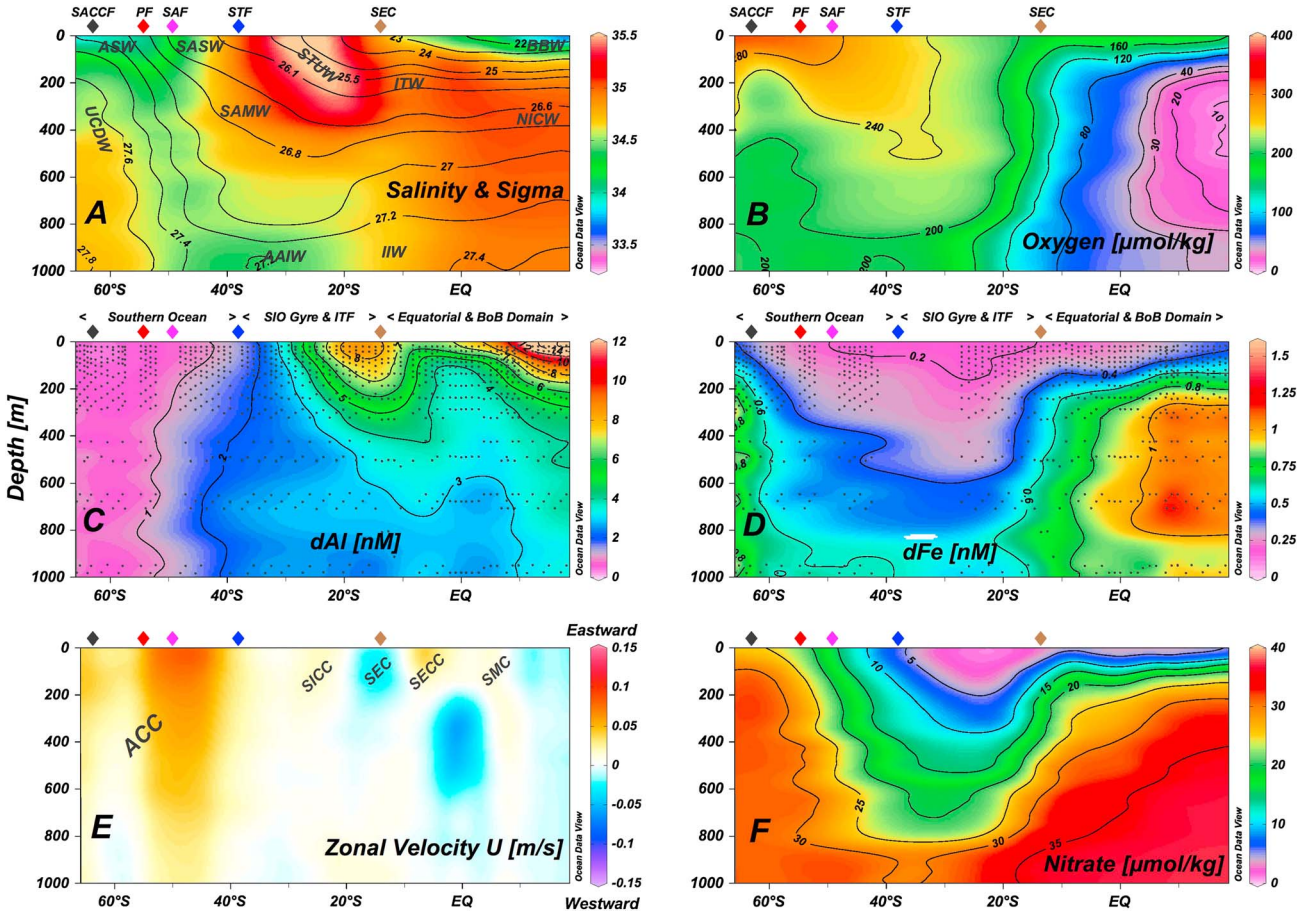

Figure 2. Property distributions along the CLIVAR I08S and I09N cruise tracks contoured using Ocean Data View 4.6.2 [*Schlitzer,* 2014]. (a) Salinity with overlaid potential density contours (σ_0), (b) dissolved oxygen (µmol kg^{-1}), (c): dAl (n*M*), (d) dFe (n*M*), (e) LADCP zonal velocity (m s^{-1}), and (f) nitrate (µmol kg^{-1}). Note that the color bar of the dAl plot only ranges from 0 to 12 n*M* (compared to the observed range of 0.3–32.35 n*M*) to minimize loss of detail at the lowest dAl levels (Figure 2c). We also altered the linearity of the color mapping scale of the dFe contour plot to reveal details of the distribution in the Bay of Bengal (Figure 2d). The colored diamonds show the position of the Southern Ocean fronts (see text) and South Equatorial Current (brown diamond). ASW: Antarctic Surface Water; SASW: Subantarctic Surface Water; UCDW: Upper Circumpolar Deep Water; AAIW: Antarctic Intermediate Water; SAMW: Subantarctic Mode Water; STUW: Subtropical Under Water; ITW: Indonesian Throughflow Water; IIW: Indonesian Intermediate Water; BBW: Bay of Bengal Water; NICW: North Indian Central Water; ACC: Antarctic Circumpolar Current; SICC: South Indian Counter Current; SEC: South Equatorial Current; SECC: South Equatorial Counter Current; SMC: Southwest Monsoon Current; SIO Gyre: South Indian Ocean Gyre; ITF: Indonesian Throughflow.

3. Results and Discussion

We subdivide the cruise track into three hydrographic regimes: the Southern Ocean domain (65.8°S–38°S), the south Indian subtropical gyre and Indonesian Throughflow plume (38°S–15°S), and the northern Indian Ocean and Bay of Bengal regime (15°S–18°N). Contour plots of salinity, oxygen, dAl, dFe, LADCP zonal velocity, and nitrate are shown in Figure 2 along with the position of the principal water masses, fronts, and currents identified on the I08S and I09N transects. All acronyms used in this paper that refer to the water masses, currents, and hydrographic provinces are defined in the captions of Figures 1 and 2.

The most striking features in the dAl distribution are the uniformly low values characterizing the Southern Ocean domain (≤1 n*M*), the sharp concentration gradient in dAl below 100 m at the northern boundary of the Southern Ocean near 45.5°S, and two regions of elevated dAl at the northern edge of the south Indian subtropical gyre and in the BoB (Figure 2c). The distribution of dFe shows an entirely different pattern across the section (Figure 2d). Elevated dFe values were measured in the immediate vicinity of the Antarctic shelf (up to 1.67 n*M*) and below 200 m beginning at the SEC and extending to the BoB (Figure 2d), where dFe concentrations were greater than 1 n*M* from 300 to 700 m with maximum concentrations east of Sri Lanka (~8°N–10°N). The lowest dFe levels were observed throughout the water column of the south Indian subtropical gyre (Figure 2d).

In the following section, we describe the circulation, water masses, and other relevant hydrographic features in relation to the distribution of dFe and dAl in the upper 1000 m of each hydrographic domain. We will discuss the most striking features of the dAl and dFe distributions, their most probable origins, and biogeochemical implications starting from the Southern Ocean domain (65.8°S–38°S) and ending at the northernmost stations in the BoB (18°N).

3.1. Southern Ocean Domain (65.8°S–38°S)

3.1.1. Oceanographic Setting

The eastward flowing Antarctic Circumpolar Current (ACC) governs the circulation of the Southern Ocean domain. In our study area, the ACC circulation is greatly impacted by the shallow topography (<2000 m) of the Kerguelen Plateau (Figure 1), which constitutes a major barrier to the ACC. According to *Park et al.* [2009], about 60% of the total ACC transport passes north of Kerguelen Island. The remaining 40% is mostly channeled through Fawn Trough, a deep gap (~2650 m) which divides the Kerguelen Plateau into the northern and southern plateaus near 56°S (Figure 1). The ACC flow is concentrated in three main fronts that were identified using the property criteria of *Orsi et al.* [1995]. These fronts separate zones with relatively uniform temperature/salinity (T/S) and macronutrient properties. The Southern Ocean domain is bounded to the north by the Subtropical Front (STF) near 38°S, whose position varies between basins and is sometimes more poorly defined than the principal ACC fronts, and to the south by the Southern Boundary (SB), which appears to merge with the South ACC front (SACCF) near 63°S on the I08S section (Figure 1). The Subantarctic Front (SAF), the strongest jet of the ACC flow field, was positioned near 49°S. The Polar Front (PF) was placed in a band spanning 3° of latitude (57°S–54°S) because a great deal of variability obscured its positioning using the subsurface temperature criterion of *Orsi et al.* [1995]. We note that similar ambiguity in defining the location of the PF was also reported during a previous occupation of the I08S transect [*McCartney and Donohue*, 2007]. While this could reflect multiple filaments of the PF, the variability in properties could also be related to the large poleward meander of the PF downstream of the Kerguelen Plateau and the eddy-rich flow field of the Polar Frontal Zone [*Belkin and Gordon*, 1996; *McCartney and Donohue*, 2007]. The ACC fronts separate four zones [*Talley et al.,* 2011]: the Southern Zone (SZ) poleward of the SACCF, the Antarctic Zone (AZ) between the SACCF and the northern branch of the PF (54°S), the Polar Frontal Zone (PFZ) from the PF to the SAF, and the Subantarctic Zone (SAZ), which extends from the SAF to the STF (Figures 1 and 2).

Antarctic Surface Water (ASW) and Subantarctic Surface Water (SASW) occupy the upper ocean south of the PF and north of the SAF (Figure 2a), respectively [*Talley et al.,* 2011]. The transition from ASW to SASW is accompanied by an increase in salinity, a gradual drop in oxygen and nitrate concentrations, a near-complete depletion of dissolved silica and a northward decrease in surface dFe from 0.46 ± 0.22 n*M* ($n = 5$) in the SZ, 0.23 ± 0.10 n*M* ($n = 8$) in the AZ, to 0.17 ± 0.06 n*M* ($n = 10$) in the PFZ&SAZ. Intermediate-depth water masses in this region include Upper Circumpolar Deep Water (UCDW) and Antarctic Intermediate Water (AAIW). UCDW shoals to about 100 m near the SACCF and has origins in the deep Pacific and Indian oceans [*Whitworth and Nowlin*, 1987; *Orsi et al.,* 1995]. UCDW is the subsurface oxygen minimum (<180 μmol kg^{-1}) lying at density values 27.35 kg m^{-3} < σ_θ < 27.75 kg m^{-3}, which shoals to about 150 m between the SACCF and the southern branch of the PF (57°S). It can be visualized as the tongue of elevated nitrate poleward of the 30 μ*M* nitrate contour (Figure 2f). On this section, the mean dFe concentration of UCDW was 0.51 ± 0.16 n*M* (mean ± 1 SD, $n = 19$), comparable to the 0.4–0.5 n*M* dFe range reported in other sectors of the Southern Ocean [*Hoppema et al.,* 2003 and references therein]. The core of the low salinity AAIW is centered at $\sigma_\theta = 27.2$ kg m^{-3} and is found between the SAF and the northern reaches of the south Indian subtropical gyre [*Fine*, 1993; *Wong*, 2005].

3.1.2. Advection of dAl Enriched Waters From the Agulhas Region

Except in the SZ, where dAl values reached up to 2.1 n*M*, the concentration of dAl in the Southern Ocean poleward of the SAF was uniformly low with values generally below 1 n*M* in the upper 1000 m (Figure 2c). In fact, in the Southern Ocean (65.8°S–38°S), 55 samples out of 287 (~19%) had dAl levels equal to or less than the analytical detection limit (~0.3 n*M*). From the SACCF to the SAF, the dAl profiles were nearly featureless, exhibiting only small concentration gradients from the surface to 1000 m. A surface dAl maximum and a subsurface minimum were observed in some profiles [e.g., *Middag et al.,* 2011], but this was not a consistent feature and the differences were not significantly greater than the analytical uncertainty. Our data confirm that dAl concentrations in the Southern Ocean are among the lowest found in the global ocean with values typically less than 1 n*M* throughout the main thermocline (Figure 2c). *Middag et al.* [2011] report dAl in the

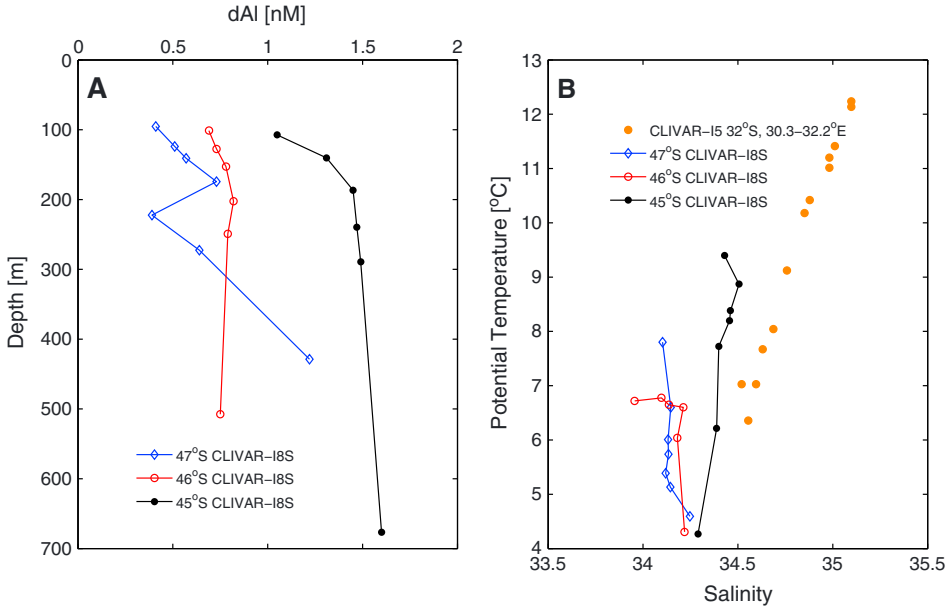

Figure 3. (a) Vertical dAl profiles at three CLIVAR I08S stations across the dAl concentration gradient (47°S–45°S) at the northern edge of the Southern Ocean domain. (b) T/S properties from the three CLIVAR I08S stations and from the CLIVAR I05 section in the Agulhas Current region along the South African shelf (32°S, 30.3°E–32.2°E), where the dAl enrichment seen on the present section may originate. Only data within the density intervals $\sigma_\theta = 26.6–27.2$ kg m^{-3} (>100 m) are included in these plots.

upper 1000 m of the ACC along the Greenwich meridian averaging 0.74 ± 0.44 n*M* (±1 SD, $n = 94$), which matches our mean dAl concentration of 0.79 ± 0.60 n*M* ($n = 229$) from all ACC stations in this study. Surface dAl (<25 m) from the Antarctic margin to the STF was 0.54 ± 0.25 n*M* ($n = 25$), comparable to previous reports near the Greenwich meridian (0.71 ± 0.43 n*M* [*Middag et al.*, 2011]), Drake Passage (0.39 ± 0.21 n*M* [*Middag et al.*, 2012]), and southeast of New Zealand (0.38 ± 0.05 n*M* [*Measures and Vink*, 2000]). The low dAl levels that characterize the remote Southern Ocean reflect the negligible mineral dust inputs impacting the surface of the circumpolar ocean [*Grand et al.*, 2015] and the subsequent subduction of these dAl-depleted water masses into the ocean interior. The lack of a significant margin imprint of dAl compared to dFe has been previously observed near Drake Passage [*Hatta et al.,* 2013; *Measures et al.,* 2013]. Whether this is a result of the inhibiting effect of elevated Si levels on dAl release from resuspended shelf sediments in Antarctic regions [*Van Hulten et al.,* 2014] is unknown at this time.

The most striking feature in the dAl distribution in the eastern Indian sector of the Southern Ocean (>38°S) is the sharp dAl concentration gradient below 100 m between the SAF and the STF (Figure 2c). A closer look at three vertical dAl profiles sampled within this region from 47°S to 45°S shows that dAl levels below 100 m increase by more than 0.5 n*M* over a degree of latitude (Figure 3a). In the Crozet Basin near 60°E, *van Beusekom et al.* [1997] observed a meridional trend in unfiltered Al that is strikingly similar to the one we observed, that is, low Al values (<1 n*M*) throughout the water column poleward of 50°S and a sharp front near 45°S separating Al-depleted circumpolar waters from Al-rich subtropical waters (>4 n*M*). At the Crozet Basin and along the present section, the transition from low to high Al waters was accompanied by a significant increase in salinity and potential temperature (Figure 3b), suggesting that the meridional increase in dAl concentrations is the product of advected subtropical waters. In the Crozet region, *van Beusekom et al.* [1997] attributed the sharp meridional increase in Al to the Agulhas Return Current and speculated that this current carries waters imprinted with a dust signal between Africa to the Crozet Basin, which would be preserved due to minimal scavenging removal along the transport pathway. An advected dAl signal emanating from Africa is consistent with the adjusted steric height maps of *Reid* [2003]. These maps display streamlines flowing southward along the east coast of Africa as part of the Agulhas Current system, which then loop eastward along the latitudinal band (~45°S–40°S) where we observed the discontinuity in the dAl distribution (Figures 2c and 3a). Recent data from seven stations of the CLIVAR I05 section

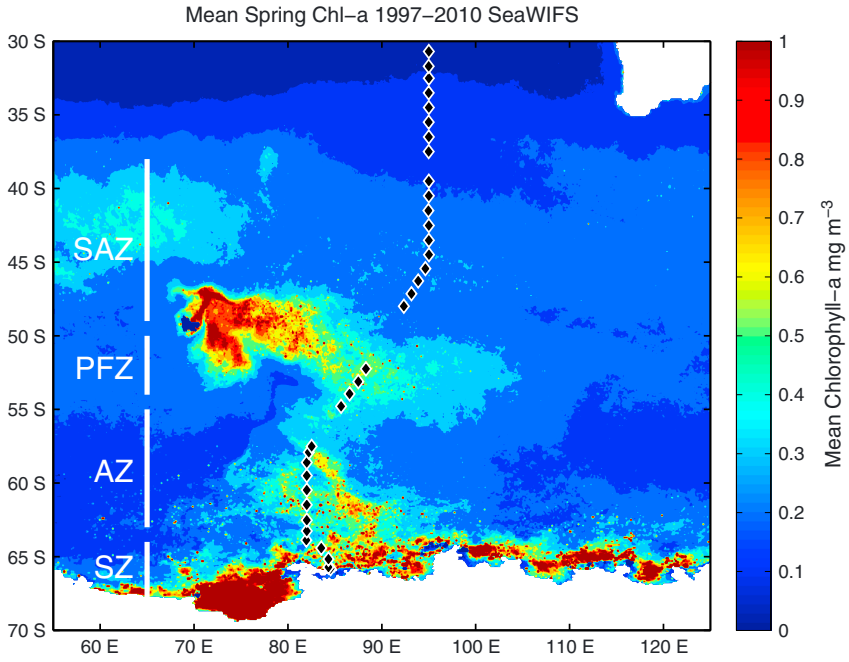

Figure 4. Mean climatological austral spring (October–December) surface chlorophyll-*a* levels (mg m^{-3}) from 1997 to 2010 in the southeast Indian Ocean based on SeaWiFS satellite imagery. The black diamonds show trace metal stations sampled on the I08S cruise track. SeaWiFS data retrieved from http://oceanwatch.pifsc.noaa.gov.

(M. M. Grand et al., The impact of circulation and dust deposition in controlling the distributions of dissolved Fe and Al in the south Indian subtropical gyre, manuscript in preparation, 2015) that crossed the *Reid* [2003] streamlines in the Agulhas Current along 32°S and 30.3°E–32.2°E showed that the mean dAl concentrations were 4.5 ± 0.9 n*M* and 3.0 ± 0.3 n*M*, between potential density contours 26.6–26.8 and 26.8–27.2 kg m^{-3}, respectively. We measured 1.5 ± 0.5 and 2.1 ± 0.6 n*M* dAl within the same density intervals at seven stations just north of the dAl concentration gradient (>46°S). Figure 3b also shows that the T/S properties of the CLIVAR I08S stations where the gradient in dAl occurs tend to approach the linear T/S properties of the central waters observed during the CLIVAR I05 section between σ_θ = 26.6–27.2 kg m^{-3} near the south African shelf. Therefore, the sharp increase in dAl concentrations observed at ~45°S along 95°E seems consistent with a dAl signal eroded via mixing and scavenging processes that originated from the Agulhas Current region. Although *van Beusekom et al.* [1997] attributed the dAl enrichment at the edge of the Southern Ocean domain to a subducted and advected dust signal, it is also possible that the resuspension of shelf sediments along the advective pathway of the Agulhas Current along the coast of Africa contributes to the dAl enrichment observed along our cruise track.

3.1.3. Elevated Subsurface dFe South of the Polar Front

Figure 4 shows the mean austral spring (October–December) surface chlorophyll-*a* levels from 1997 to 2007 based on Sea-viewing Wide Field-of-view Sensor (SeaWiFS) imagery in the eastern Indian sector of the Southern Ocean. This satellite chlorophyll-*a* climatology and the recent model estimates of net primary productivity of *Takao et al.* [2012] show that the I08S cruise track transected two anomalously productive sectors of the high-nutrient low-chlorophyll (HNLC) Southern Ocean. The first extends from the Antarctic margin until the ice limit defined by *Park et al.* [1998] near 56°S–58°S and is possibly fueled by the advection of Antarctic waters from the south carrying biomass and nutrients along the western flank of the southern Kerguelen Plateau [*Rintoul et al.*, 2008]. The second productive zone, north of PF, has been attributed to natural Fe fertilization, with the Fe supplied via resuspension of shelf sediments and lateral transport of waters that have been in contact with the plateau's sediments [*Blain et al.*, 2008; *Chever et al.*, 2010]. In the following, we compare our mean Southern Ocean dFe concentrations with historical observations and then discuss the principal sources of dFe in relation to the circulation and productivity patterns that characterize our study area (Figure 4).

Table 1. Dissolved Fe (dFe) Statistics (mean ± 1 SD) South and North of the Polar Front From This Study Compared With a Recent Compilation of Historical Observations in the Indian Sector of the Southern Ocean[a]

	Depth Range (m)	This Study	Database[b]
AZ(<54°S)	0–100	0.34 ± 0.15	0.43 ± 0.51
	100–500	0.64 ± 0.28	0.32 ± 0.24
	500–1000	0.69 ± 0.22	0.28 ± 0.14
PFZ&SAZ(54°S–38°S)	0–100	0.18 ± 0.10	0.23 ± 0.20
	100–500	0.27 ± 0.11	0.24 ± 0.19
	500–1000	0.53 ± 0.12	0.30 ± 0.11

[a]AZ: Antarctic Zone; PFZ&SAZ: Polar Frontal Zone and Subantarctic Zone.
[b]*Tagliabue et al.* [2012].

Table 1 lists the mean dFe values observed south and north of the northern branch of the PF (54°S) along with the measurement compilation statistics of *Tagliabue et al.* [2012] for the Indian sector of the Southern Ocean (20°E–180°E). Note that seven stations with a bottom depth shallower than 2000 m (near the Antarctic margin and above the southern extension of the Kerguelen Plateau near 60°S) were excluded from the statistics displayed in Table 1 to ensure a meaningful comparison with the definition of "off-shelf" used in the database of *Tagliabue et al.* [2012]. On the I08S transect, the mean dFe concentrations in the upper (0–100 m), intermediate (100–500 m), and deep (500–1000 m) depth intervals were significantly higher in the Antarctic Zone (AZ) than in the Polar Frontal Zone and Subantarctic Zone combined (PFZ&SAZ; Mann–Whitney *U* test, $p < 0.05$). This overall trend of decreasing dFe concentrations to the north in surface and intermediate waters is consistent with the aforementioned database (Table 1). However, our mean dFe concentrations were more than twice those of the database in AZ waters deeper than 100 m and also in the deepest depth interval of the PFZ&SAZ (500–1000 m; Table 1). This database does not include the region of our cruise track above and downstream of the Kerguelen Plateau, which, as we discuss later, is the most likely source for this subsurface dFe enhancement.

Poleward of the PF, potential dFe sources to the upper layers include sedimentary inputs [*Dulaiova et al.,* 2009; *Ardelan et al.,* 2010; *de Jong et al.,* 2012; *Measures et al.,* 2013; *Hatta et al.,* 2013; *Klunder et al.*, 2014], the seasonal melting of sea ice and icebergs enriched in dFe from shelf and dust inputs [*Lannuzel et al.,* 2007, 2010; *Lin et al.*, 2011], and upwelling inputs from deep waters [*de Baar et al.*, 1995; *Croot et al.,* 2004; *Klunder et al.,* 2011]. The latter process may lift the ferricline to shallower depths [*Sokolov and Rintoul*, 2007; *Boyd and Ellwood*, 2010], thereby facilitating the entrainment of dFe-rich deep waters into the euphotic zone during deep winter mixing [*Nishioka et al.,* 2011*; Tagliabue et al.*, 2014b]. Dust deposition is a negligible source of dFe to surface waters of the Southern Ocean domain [*Tagliabue et al.,* 2014a]. Indeed, using mixed layer dAl data from our cruise track and a modified version of the Measurement of Al for Dust Calculations in Oceanic Waters model (MADCOW) [*Measures and Brown*, 1996; *Grand et al.*, 2015] calculated that the dissolution of mineral dust could supply 1.2 ± 1.1 μmol m^{-2} yr^{-1} of dFe to surface waters of the Southern Ocean domain. This aeolian flux is small relative to the mean dFe inventory (12 ± 5 μmol m^{-2}, $n = 23$) observed in the mixed layer (53 ± 20 m, $n = 23$) of our Southern Ocean domain and nearly 20 times smaller than the mean winter entrainment pulse of dFe (21.1 μmol m^{-2} yr^{-1}) recently estimated for the Southern Ocean [*Tagliabue et al.,* 2014b].

Poleward of the SACCF (63°S), in the Southern Zone (SZ), the most important dFe sources are most likely shelf inputs from the Antarctic margin at depth and the seasonal melting of fast ice and grounded icebergs near the surface. Elevated dFe concentrations (0.64–1.67 n*M*) were observed at all depths at the two stations closest to the Antarctic shelf (bottom depth 450 m), consistent with previous observations in other Antarctic sectors that attributed enhanced dFe to shelf sediments [*Sohrin et al.,* 2000; *Sedwick et al.,* 2008; *Klunder et al.,* 2011; *Hatta et al.,* 2013; *Measures et al.,* 2013]. Two lines of evidence support the existence of sedimentary Fe inputs in the SZ. The first is the absence of correlation between dFe and apparent oxygen utilization (AOU) from the base of the mixed layer to the depth of the oxygen minimum in the dense and cold waters of the SZ ($\sigma_0 > 27.5$ kg m^{-3}, $\theta < 0$°C), implying that remineralization processes are not the sole source of dFe there (data not shown). In contrast, dFe and AOU are linearly correlated farther north in the AZ and PFZ&SAZ, suggesting that sedimentary dFe inputs in these regions do not overwhelm the dFe signal resulting from the remineralization of organic matter (data not shown). The second is that unlike any other region sampled along the cruise track, dAl and dFe were positively correlated throughout the water column of the SZ ($R^2 = 0.68$, $n = 44$; Figure 5). This correlation implies that a common process, presumably of sedimentary origin, regulated their distributions (Figure 5). The surface freshening (Figure 2a) and elevated yet spatially variable dFe concentrations (0.46 ± 0.22 n*M*, $n = 5$) observed at all stations of the SZ suggest that the melting

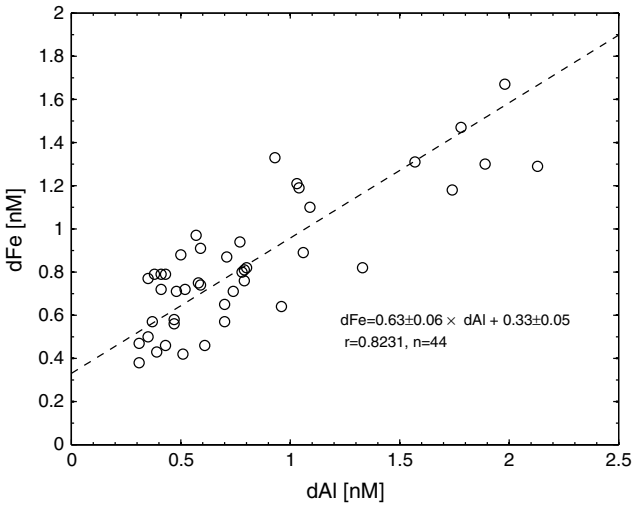

Figure 5. Dissolved Fe versus dissolved Al in the Southern Zone, poleward of the SACCF (<63°S). The dashed line and equation were produced based on a Type II regression between dFe and dAl (reduced major axis method). Note that 13 samples with dAl less than the instrumental detection limit (0.3 n*M*) were neither plotted nor included in the regression analysis.

of fast ice and grounded icebergs enriched in particulate and dissolved Fe is another possible source of dFe to surface waters of the SZ [*Lannuzel et al.,* 2007, 2010, 2014].

Farther north, in the AZ, two mechanisms related to the interaction of the ACC with the shallow topography of the southern Kerguelen Plateau may be invoked to explain the anomalously elevated dFe concentrations that we observed deeper than 100 m (Table 1). The first mechanisms involve the northward meander that the ACC executes around the western flank of the Kerguelen Plateau prior to passing through the Fawn Trough (Figure 1), which truncates the southern and northern portions of the Kerguelen Plateau near 56°S, 78°E [*Rintoul et al.,* 2008; *Roquet et al.,* 2009]. In their investigations of the origin of the large sea ice tongue that recurrently forms near 85°E above the southern Kerguelen Plateau, *Rintoul et al.* [2008] observed and modeled strong northward currents near 85°E that likely carry sea ice and waters from the SZ to the latitude of the Fawn Trough (Figure 1). Offshore flow near 85°E may also carry dFe-enriched waters northward, which, as we showed above, likely received dFe from shelf sediments at depth (Figure 5) and ice melt inputs near the surface. The second mechanism that may contribute to the elevated dFe observed below the mixed layer in the AZ revolves around the possibility of enhanced upwelling above the southern Kerguelen Plateau due to the bottom pressure torque that results from the interaction of the ACC with the shallow bathymetry (<2000 m) of the plateau [*Sokolov and Rintoul,* 2007] and/or enhanced vertical mixing associated with strong internal tides [*Park et al.,* 2008]. Such processes may enhance the uplift of dFe-rich deep waters to shallower depths, thereby contributing to the anomalously elevated values that we observed deeper than 100 m in the AZ relative to other Southern Ocean regions devoid of shallow bathymetry (Table 1). In this regard, it is worth noting that the recurrent annual blooms observed in the vicinity of major bathymetric features around the Southern Ocean (including our study region across Kerguelen Plateau) appear to coincide with model outputs of enhanced vertical velocities [*Sokolov and Rintoul*, 2007]. This observation suggests that topographic upwelling is an important process that could supply deep dFe to the upper layers and fuel the hot spots of productivity observed near bathymetry along the flow path of the ACC. In summary, we speculate that the offshore advection of dFe rich waters from the SZ near 85°E and enhanced upwelling above the southern Kerguelen Plateau are likely to sustain the elevated dFe values that we observed below the mixed layer in the AZ of our cruise track. The entrainment of these dFe-rich subsurface waters into the euphotic zone during deep winter mixing [*Measures and Vink*, 2001; *Tagliabue et al.,* 2014b] may also contribute to the hot spot of productivity that characterize the AZ of our cruise track in austral spring (Figure 4).

3.1.4. Elevated Subsurface dFe in the PFZ-SAZ Downstream of Kerguelen Plateau

The Kerguelen bloom is one of the largest recurrent blooms of the Southern Ocean and appears to be fueled in dFe via lateral transport of waters that have been in contact with the plateau's sediments as well as enhanced vertical mixing of dFe-rich deeper waters [*Moore and Abbott*, 2000; *Chever et al.,* 2010; *Park et al.,* 2008]. The bloom typically extends 1000–2000 km downstream of the Kerguelen Fe source in a matter of weeks, which is much shorter than the 2–3 month period required for transport by the ACC over such a distance [*Mongin et al.*, 2009]. This excludes the possibility that the spatial extent of the Kerguelen Bloom is simply a product of advection and suggests that there is potentially enough dFe of Kerguelen origin advected during the unproductive winter season to produce and sustain the bloom when favorable light and stratification conditions return [*Mongin et al.,* 2009].

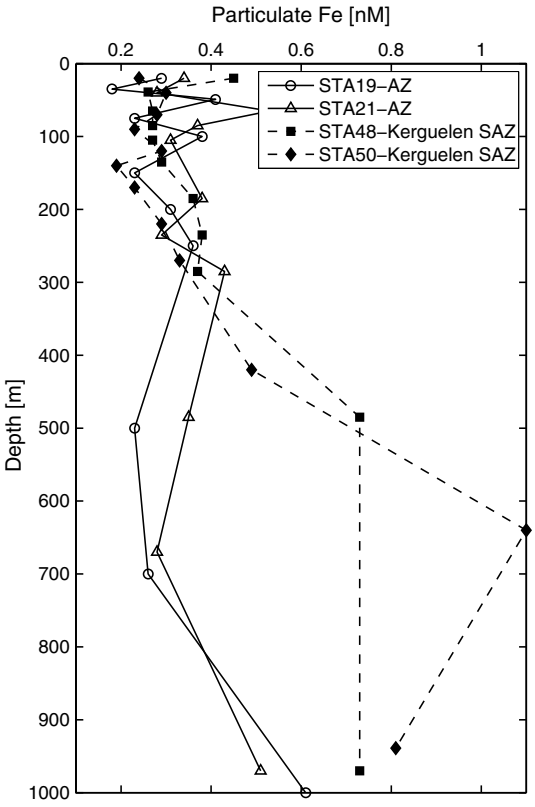

Figure 6. Particulate Fe (>0.4 μm) profiles in the Antarctic Zone (AZ) and in the Subantarctic Zone (SAZ) downstream of the Kerguelen Plateau. Note the elevated subsurface pFe values >300 m at the two stations downstream of Kerguelen Plateau. Particulate Fe concentrations determined by ED-XRF as in *Barrett et al.* [2012].

The PFZ&SAZ sampled in this study encompasses four stations located ~1500 km southeast of the naturally Fe fertilized area of the Kerguelen-Heard Plateau [*Blain et al.,* 2008]. We observed a great deal of variability in the vertical dFe profiles and T/S plots at the four PFZ stations that were within the annual Kerguelen bloom (Figure S1 in the supporting information). This variability may reflect the presence of a dense field of mesoscale eddies spanning across the PFZ-SAZ inferred from sea surface height altimetry maps of February 2007 (Figure S2). Our mean dFe values in the PFZ-SAZ compare well with the database of *Tagliabue et al.* [2012], except in the 500–1000 m depth interval, where our values were significantly higher (Table 1). Several processes may act in concert to produce elevated deep dFe levels (500–1000 m) on our cruise track, downstream of the Kerguelen Plateau. In the first, discussed previously, interaction of the ACC with the Kerguelen Plateau could enhance vertical mixing [*Sokolov and Rintoul,* 2007; *Park et al.,* 2008]. This may entrain dFe-rich waters to shallower depths and this anomaly could be propagated ~1500 km to our cruise track [*Sokolov and Rintoul*, 2007]. It is also possible that a sedimentary signal emanating from the Kerguelen Plateau's sediments is advected to our cruise track. In this regard, the particulate Fe profiles (>0.4 μm) measured on the cruise show a distinct tongue of elevated particulate Fe centered near 50°S and deeper than 300 m in the SAZ downstream of Kerguelen Plateau relative to stations sampled in the AZ near Fawn Trough (Figure 6). It would take approximately 87–174 days for a water mass in contact with the plateau's sediments to travel the ~1500 km separating the plateau from our cruise track assuming an eastward ACC flow of 0.1–0.2 m s^{-1} below 500 m in the PFZ-SAZ. Considering that the residence time of pFe in SAZ waters southeast of New Zealand was estimated to be on the order of 100 days [*Frew et al.,* 2006], it is conceivable that the remnants of a particulate and dFe signal emanating from the plateau's sediments could be transported and detected along our cruise track. Finally, organic matter remineralization could also contribute to the elevated subsurface dFe observed in the PFZ-SAZ since we sampled the region in late February at the end of the annual Kerguelen bloom when surface chlorophyll-*a* levels had returned to background levels (<0.3 mg m^{-3}).

3.2. Subtropical Gyre and Indonesian Throughflow Plume (38°S–15°S)

3.2.1. Oceanographic Setting

We define the south Indian subtropical gyre as the region extending from the Subtropical Front (STF) to the westward flowing South Equatorial Current (SEC) near 15°S (Figure 1). The circulation in the upper 200 m of the central gyre is dominated by the northeastward flowing South Indian Counter Current (SICC) and conforms to the anticyclonic gyral circulation deeper than 200 m [*Reid*, 2003; *Siedler et al.*, 2006; *Talley et al.,* 2011]. The upper thermocline is composed of Subtropical Underwater (STUW), characterized by an equatorward spreading salinity maximum in the upper 300 m of the gyre (Figure 2a). In the southern reaches of the gyre at the base of the STUW, Subantarctic Mode Water (SAMW) occupies the water column between σ_θ = 26.6 and 26.8 kg m^{-3} (Figure 2a). SAMW is a product of the Southern Ocean subantarctic zone and is formed during deep winter convection. This process yields a thick water mass of relatively uniform

properties that is subducted northward into the subtropical gyre. On this section, we sampled the densest variety of SAMW (also known as Southeast Indian Subantarctic Mode Water (SEISAMW)), which probably originated from the subantarctic region south of Australia [*Karstensen and Tomczak*, 1997; *Wong,* 2005; *Koch-Larrouy et al.*, 2010]. Below the SAMW and deeper than 750 m lies the characteristic salinity minimum of AAIW, which extends to about 20°S in the gyre (Figure 2a).

At the northern end of the gyre, the SEC carries low-salinity waters of the Indonesian Throughflow (ITF) westward at surface and intermediate depths across the Indian Ocean [*Gordon et al.,* 1997; *Schott and McCreary*, 2001; *Talley and Sprintall*, 2005]. On this section, the ITF outflow was associated with a sharp surface salinity front near 15°S (Figure 2a), a well-defined zone of westward velocities in the upper 200 m (Figure 2e) and a bullet of fresh and silica-rich (>80 μ*M*) waters extending from 15°S to 11°S at intermediate depths (>800 m), which characterizes Indonesian Intermediate Water (IIW). The upper ITF layer is commonly referred to as Indonesian Throughflow Water (ITW) and fills the upper 400 m of the water column. Note that this water mass is also referred to as Australasian Mediterranean Water (AAMW [*You and Tomczak*, 1993]) but we use the more recent ITW naming convention, which is more explicit in terms of its source region.

3.2.2. Australian Dust Deposition and Indonesian Throughflow

The most striking feature in the subtropical dAl distribution is the region of elevated values (>4 n*M*) centered near 18°S and extending from the surface to about 400 m at the northern edge of gyre (Figure 2c). The surface maxima (up to 11.7 n*M*) of all vertical dAl profiles in this region result from the deposition and dissolution of mineral dust emanating from Australia [*Grand et al.*, 2015]. This signal is then injected into the upper 200 m of the gyre via subduction along outcropping isopycnals from ~25°S to 18°S (Figures 2a and 2c). Low scavenging rates arising from the low productivity of the south Indian gyre likely play a role in the maintenance of this zone of elevated dAl, consistent with the lack of pronounced subsurface dAl minima in the vertical dAl profiles of the gyre.

The elevated dAl concentrations observed at the northern limb of the south Indian subtropical gyre may also reflect the lateral advection of ITF waters (Figure 2c), which are imprinted with a significant surface ^{228}Ra signal from shelf sediments and a specific surface rare earth element pattern sourced from the Pacific and Indonesian Seas [*Nozaki and Yamamoto,* 2001; *Alibo and Nozaki*, 2004]. In particular, the outflow of ITF waters could be invoked to explain the origin of the elevated dAl levels (>4 n*M*) observed below 200 m ($\sigma_\theta > 25.5$ kg m^{-3}) from 20°S to 10°S, which cannot be a product of subduction since the isopycnals occupying this depth range outcrop south of 30°S where the surface dAl concentrations were less than 4 n*M* (Figure 2c). In this regard, we note that some of the highest dAl concentrations of the gyre overlap with the position of the westward flowing SEC (Figures 2c and 2e). In addition, the sharp decline in dAl at the northern boundary of the region of elevated dAl near 10°S coincides with a reversal in LADCP current velocities, marking the transition from the westward flowing SEC to the eastward flowing South Equatorial Counter Current (SECC; Figure 2e). If the lateral transport of ITF waters was the principal source of dAl at the northern limb of the south Indian subtropical gyre, one would expect to observe a negative gradient in dAl concentrations from the ITF outflow to our cruise track because some of the dAl should be lost via mixing and scavenging processes along the flow path of the SEC. However, our dAl concentrations within the core of the SEC at 12.5°S were generally higher than the soluble Al data (<0.04 μm) of *Obata et al.* [2004] collected near the ITF outflow at 12.5°S, 117°E (Figure S3). This may result from interannual variations in the strength or interaction of the ITF with sediments between the 10 years that separated our sampling from that of *Obata et al.* [2004]. More observations in the Indonesian seas and along the advective flow path of the SEC are needed to investigate the potential role of the ITF in supplying dAl and perhaps other trace elements across the northern limb of the south Indian subtropical gyre.

Deep dAl values were relatively uniform across the gyre and ITF plume region with a mean concentration of 2.5 ± 0.3 n*M* ($n = 20$, >980 m). The only other published dAl data in the south Indian subtropical gyre were collected at two stations located 20–30 degrees west of our cruise track as part of the GEOTRACES-Japan expedition in December 2009 [*Vu and Sohrin*, 2013]. In the 500–1000 m depth interval, where temporal variations in dAl should be negligible on a 2 year timescale, *Vu and Sohrin* [2013] reported a mean dAl of 2.65 ± 0.48 ($n = 6$), which is virtually identical to the mean dAl (2.63 ± 0.35 n*M*; $n = 42$) we observed in the same depth range in the gyre (38°S to 15°S) along 95°E.

Unlike dAl, the distribution of dFe in the gyre did not show enrichment associated with the deposition and dissolution of mineral dust originating from Australia. In fact, the lowest dFe values of the entire section were measured throughout the water column of the central subtropical gyre, where dFe levels remained below 0.3 n*M* in the upper 500 m. This region overlaps with the saltiest near-surface waters observed in the region (i.e., STUW) and the most intense depletion of nitrate observed in the upper 300 m of the section (Figure 2f). *Grand et al.* [2015] suggested that the lack of dFe enrichment in the upper layers of the gyre is likely due to its short residence time in surface waters (~0.6 years), which is shorter than the 0.7 year that separates the most recent Australian dust inputs and our sampling. The low dFe concentrations observed at depth are consistent with the low productivity of the gyre surface waters, resulting in negligible subsurface remineralization inputs of dFe. Our mean dFe from 500 to 1000 m in the gyre (0.47 ± 0.13, $n = 21$) is virtually identical to that observed by *Vu and Sohrin* [2013] at the two GEOTRACES-Japan stations ER-10 and ER-11 sampled west of our cruise track (0.48 ± 0.13, $n = 6$) but is higher than the initial shipboard values reported by *Nishioka et al.* [2013] at the same stations analyzed via shipboard FIA (0.30 ± 0.09, $n = 6$).

3.3. The Northern Indian Ocean and Bay of Bengal (15°S–18°N)

3.3.1. Oceanographic Setting

The position of the SEC near 15°S coincides with a remarkable biogeochemical front across the upper 1000 m of the water column, separating the monsoon-dominated regime of the northern Indian Ocean from the south Indian subtropical gyre [*Gordon et al.*, 1997; *Tomczak and Godfrey*, 2003]. In the upper 100 m, the position of the SEC coincides with an abrupt decrease in salinity (Figure 2a) that intensifies in the BoB (>5°N). Below ~200 m, the SEC appears to separate dFe-rich and oxygen-depleted waters from the northern Indian Ocean from the dFe-depleted and oxygen-rich waters of the south Indian subtropical gyre (Figures 2d and 2e). The strong property gradients observed at this latitude imply little meridional transport across 15°S along the cruise track [*You and Tomczak*, 1993; *Tomczak and Godfrey*, 2003].

The principal water masses of the northeast Indian Ocean thermocline are the low-salinity Bay of Bengal Water (BBW), which overlies North Indian Central Water (NICW). Excess precipitation over evaporation and monsoonal river inputs collectively create BBW, which spreads southward across the surface of the BoB to produce a salinity gradient in the upper layers of the water column. This, combined with warm sea surface temperature, generates a strongly stratified surface layer in the BoB that impedes entrainment of nutrients from below via wind-driven mixing [*Prasanna Kumar et al.*, 2002]. The mixed layer of the BoB is thus relatively shallow (<20 m), isolated from the main thermocline and mostly nitrogen limited [*Koné et al.,* 2009], consistent with the barely detectable nitrate levels (0–0.07 μ*M*) observed at the time of our sampling. In contrast, surface silicic acid (Si) levels doubled from 5°N to 18°N as a result of increasing riverine influence, which is particularly visible in the northern reaches of the BoB (>10°N) where the lowest surface salinities (down to 32.61) and highest Si concentrations (up to 2.35 μ*M*) were observed. Surface dFe and dAl concentrations also showed a meridional concentration gradient with pronounced increases coinciding with decreasing salinity in the BoB [*Grand et al.*, 2015]. Below the BBW, NICW occupies the majority of thermocline in the north Indian Ocean [*You and Tomczak*, 1993; *You*, 1997]. NICW is an aged form of Indian Central Water (ICW), which is subducted near the STF and injected northward into the south Indian subtropical gyre. Since the jet-like inflow of the ITF suppresses meridional transport across 10°S–15°S east of 50°E, ICW is transported westward once it reaches 10°S–15°S with the SEC and enters the Northern Hemisphere along the African coast via the Somali Current during the southwest monsoon [*You and Tomczak*, 1993; *You*, 1997]. Some ICW then retroflects eastward via the Southwest Monsoon Current (SMC) and fills the BoB, where it has been renamed NICW. The thermocline of the BoB thus contains the oldest central water of the north Indian Ocean [*You and Tomczak*, 1993; *Fine et al.,* 2008], which has accumulated macronutrients and became depleted in oxygen during its transit to the northeastern Indian Ocean and BoB.

The north Indian Ocean is subjected to seasonally reversing monsoon winds, which causes a pronounced seasonality in freshwater inputs and seasonally reversing currents. LADCP data revealed a complex current structure in the upper 1000 m of the north Indian Ocean. In particular, we observed a broad subsurface region of westward velocities centered about the equator near 400 m (Figure 2e), which

could be interpreted as a deep equatorial jet or a seasonal Rossby wave. The region between the equator and Sri Lanka is a major pathway for the exchange of water between the Arabian Sea and the BoB, particularly during summer when the Southwest Monsoon Current (SMC) carries high-salinity waters of the Arabian Sea past the Sri Lanka dome before turning northward into the BoB [*Schott and McCreary,* 2001].

3.3.2. Lithogenic Inputs in Subsurface Waters of the Bay of Bengal

The distribution of dAl in the northern Indian Ocean shows an increase from south to north, with systematically higher concentrations throughout the upper 1000 m in the northern BoB (>10°N) where the highest surface (up to 32 n*M*) and deep (>800 m) dAl levels (up to 3.75 n*M*) of the entire section were observed (Figure 2c). Note that *Vu and Sohrin* [2013] sampled a station in 2009 (station ER-2) located within 30 nautical miles of one of our stations in the central BoB (8.5°N). They reported mean dAl concentrations from 0 to 100 m (8.6 ± 1.7 n*M*, $n = 4$), 100 to 500 m (4.9 ± 0.6 n*M*, $n = 3$), and 500 to 1000 m (3.6 ± 0.3 n*M*, $n = 3$) that were not significantly different from the mean values we observed within these same depth intervals (two-sample *t*-test: 0–100 m: 6.7 ± 1.9 n*M*, $n = 4$; 100–500 m: 5.2 ± 1.1 n*M*, $n = 6$; and 500–1000 m: 3.3 ± 0.4 n*M*, $n = 2$). In the stratified upper layers of the BoB, the most likely sources of dAl and dFe include dust deposition and runoff from the Ganges-Brahmaputra and peninsular Indian rivers [*Grand et al.*, 2015].

The supply of suspended particulate matter associated with the Ganges-Brahmaputra river plume is one of the largest in the world [*Milliman and Meade*, 1983] and can be traced in deep-sea sediments of the northern Indian Ocean as far as 8°S [*Nath et al.,* 1989]. The large fluvial input of particulate material throughout the BoB is well documented in sediment trap studies, which show a decreasing trend in the contribution of settling lithogenic material delivered to sediment traps at ~1000 m with increasing distance from the coast [*Unger et al.*, 2003]. The influence of riverine material in the BoB was also seen in the distribution of particulate Al and Fe measured in this section, which exhibited a remarkable meridional gradient across the northern Indian Ocean, with the highest values observed underneath the freshwater lens of the northern BoB (P. Barrett, personal communication, 2014). In this region at depths below 100 m, the ratio of particulate Fe to Al averaged 0.37 ± 0.06 (mol : mol), which is close to the mean particulate Fe : Al ratio of 0.24 (mol :mol) observed in riverborne sediments of the Ganges-Brahmaputra system [see *Subramanian et al.*, 1985, Table V]. The parallel north–south decreasing trends in dAl, particulate Al and Fe, and settling lithogenic fluxes inferred from sediment trap studies suggest that the enormous input of riverine particulate material from the Ganges-Brahmaputra and peninsular rivers likely influences the distribution of dAl and dFe throughout the BoB. While the dissolution of settling riverine particulate material has been invoked as an important source of rare earth elements below the stratified upper layer of the BoB [*Nozaki and Alibo*, 2003; *Singh et al.,* 2012], we surmise that the deposition of riverine sediments to the shelves and their subsequent resuspension in turbidity currents cascading down the slope may be an important source of dAl. These turbidity currents could release pore waters enriched in dAl thereby contributing to the elevated subsurface dAl observed in the BoB relative to other regions along the cruise track. As we will show in section 3.3.4, the subsurface distribution of dFe is also impacted by sedimentary inputs but, unlike dAl, this signal is superimposed on that produced via remineralization of settling organic matter.

3.3.3. dFe Distribution in the Sri Lanka Dome Bloom Region

East of Sri Lanka, from ~7.7°N to 9.8°N, subsurface dFe levels were enriched between ~200 and 800 m relative to other regions sampled in the BoB (Figure 2d). This zone of elevated subsurface dFe is located at the northeastern edge of the Sri Lanka dome (Figure 1), an open ocean region where deep waters are upwelled to the surface via Ekman pumping during the southwest monsoon [*Vinayachandran and Yamagata*, 1998]. This process brings deep nutrients into surface layers and generates a recurrent phytoplankton bloom, which usually peaks in June–July and extends from ~84°E to 88°E and 4°N to 10°N [*Vinayachandran et al.*, 2004]. We sampled six stations at the northeastern edge of the Sri Lanka dome (Figure 7a). These profiles exhibited variable dFe levels below 150 m and dFe concentration maxima of 1.14–1.51 n*M* located between ~300 and 650 m (Figure 7a). Since the highest subsurface dFe concentrations of the BoB coincide with the geographical extent of the Sri Lanka dome bloom (Figures 1 and 2d), it is likely that this subsurface dFe enrichment partly results from remineralization of the seasonal Sri Lanka bloom. Aeolian dFe inputs in the Sri Lanka dome bloom region, which

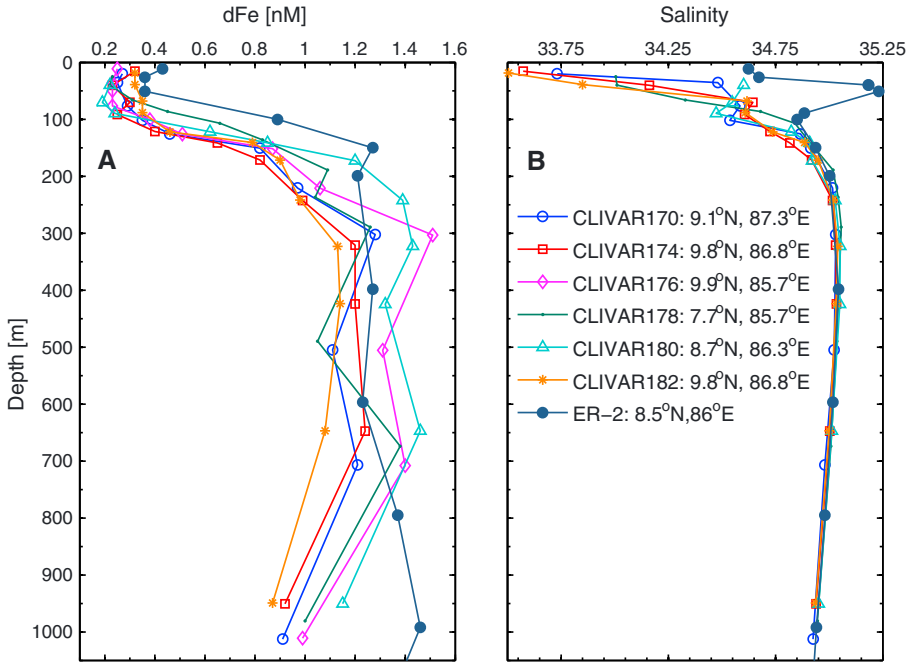

Figure 7. (a) Dissolved Fe and (b) salinity profiles from the Sri Lanka dome region observed on this section and during the GEOTRACES-Japan expedition in November 2009 (ER-2 [*Vu and Sohrin*, 2013]).

appear to be of comparable magnitude to that observed underneath the Saharan dust plume in the north Atlantic [*Grand et al.*, 2015], probably also contribute to the surface inventory of bioavailable dFe there.

The Sri Lanka dome bloom region was also sampled for dFe at GEOTRACES-Japan station ER-2 (8.5°N, 86°E) in November 2009 [*Vu and Sohrin*, 2013]. Their dFe observations were higher than ours (April 2007) in the upper 200 m and below 800 m, but were within the range of our observations between 200 and 800 m (Figure 7a). Interestingly, salinity in the upper 200 m was significantly higher during the occupation of station ER-2 (Figure 7b). The higher salinity and dFe concentrations observed in the upper 200 m of the water column during the GEOTRACES-Japan expedition may reflect an advected feature originating from the Arabian Sea or the different timing of the CLIVAR (April: prebloom) and GEOTRACES-Japan observations (November: postbloom). It would appear, however, that the elevated subsurface dFe levels that we observed underneath the Sri Lanka dome bloom may be a quasi-persistent feature of the BoB considering the relative agreement between our subsurface dFe observations and those of *Vu and Sohrin* [2013], which were sampled 2 years later and at a different season.

3.3.4. Net Remineralization Inputs Along the Pathway of Indian Central Water

The most striking characteristic of the subsurface dFe distribution in the north Indian Ocean is the pronounced increase in dFe below ~100 m starting near the SEC and extending into the BoB (Figure 2d). As mentioned previously, the southernmost extent of this zone of elevated dFe near ~15°S coincides with a sharp front in the oxygen distribution and the ensuing northward dFe increase is accompanied by declining oxygen levels (Figures 2b and 2d). The low oxygen content of these subsurface waters results from the lack of direct ventilation in the north Indian Ocean, combined with the lateral transport of oxygen deficient waters from the western Indian Ocean and in situ remineralization of sinking organic matter along their flow path. Once a water mass last comes in contact with the atmosphere and is advected away from its subduction region, it will lose oxygen and accumulate macronutrients and dFe as a result of remineralization of settling organic matter. However, unlike macronutrients such as phosphate, the subsurface distribution of dFe reflects the dynamic balance between remineralization inputs and scavenging removal and can also be impacted by inorganic inputs, which are decoupled from the remineralization and scavenging processes.

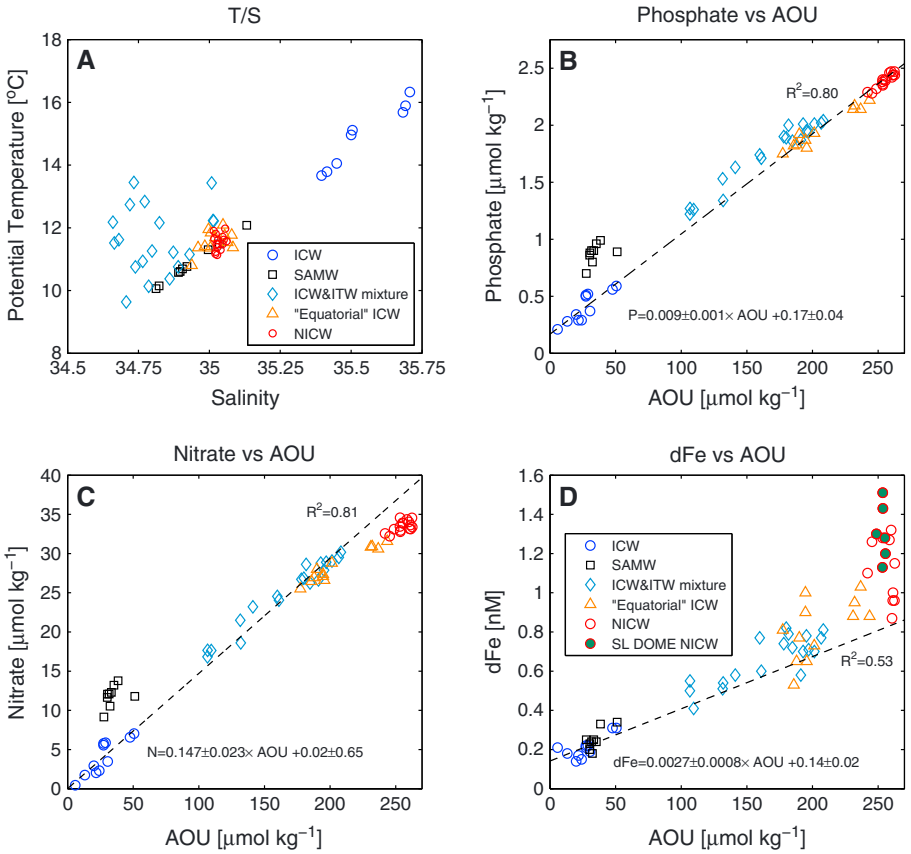

Figure 8. Remineralization dynamics along the pathway of ICW from its southernmost position in the south Indian subtropical gyre of the present section to its northernmost extent in the Bay of Bengal where it has been renamed NICW. T/S properties of (a) ICW (latitude: 27°S–16.3°S, $\sigma_\theta = 26.1–26.8\ kg\ m^{-3}$), SAMW (latitude: 27°S–16.3°S, $\sigma_\theta = 26.6–26.8\ kg\ m^{-3}$), ICW&ITW mixture (latitude: 16.3°S–7.7°S, $\sigma_\theta = 26.1–26.8\ kg\ m^{-3}$), "Equatorial" ICW (latitude: 7.7°S–6.5°N, $\sigma_\theta = 26.6–26.8\ kg\ m^{-3}$), and NICW (latitude: 6.5°N–18°N, $\sigma_\theta = 26.6–26.8\ kg\ m^{-3}$). (b) Phosphate versus AOU. The dashed line and equation show the ordinary least squares (OLS) fit of phosphate versus AOU in ICW (latitude: 27°S–16.3°S, $\sigma_\theta = 26.1–26.8\ kg\ m^{-3}$). (c) Nitrate versus AOU. The dashed line and equation show the OLS fit of nitrate versus AOU in ICW (latitude: 27°S–16.3°S, $\sigma_\theta = 26.1–26.8\ kg\ m^{-3}$). (d) Dissolved Fe versus AOU. The dashed line and equation show the OLS fit of dFe versus AOU in ICW (latitude: 27°S–16.3°S, $\sigma_\theta = 26.1–26.8\ kg\ m^{-3}$). The filled circles refer to NICW occupying the seasonally productive Sri Lanka dome.

To illuminate the role of remineralization (i.e., dFe released via remineralization of organic matter minus scavenging removal) in controlling the subsurface distribution of dFe in the thermocline of the northern Indian Ocean, it is instructive to explore the relationships between macronutrients, dFe and AOU along the advective pathway of Indian Central Water (ICW) from its southernmost position in the subtropical gyre to the northern reaches of the BoB along our cruise track. In the subtropical gyre, ICW occupies the water column from $\sigma_\theta = 26.1–26.8\ kg\ m^{-3}$. For the purposes of this analysis, we only include data north of 27°S since the dFe data from 41.5°S to 27°S were questionable and could not be verified via shore-based ICP-MS determinations (see section 2.2). In the gyre, the ICW density range ($\sigma_\theta = 26.1–26.8\ kg\ m^{-3}$) encompasses SAMW ($\sigma_\theta = 26.6–26.8\ kg\ m^{-3}$), which is situated on the T/S mixing curve of ICW (Figure 8a). From 16.3°S to 7.7°S, the T/S properties within the ICW density range show a significant freshening and large scatter because of the inflow of ITF waters (Figure 8a). The waters within this latitudinal band are thus a mixture of ICW and ITF. From 7.7°S to the northernmost stations of the BoB, we only consider data between $\sigma_\theta = 26.6$ and $26.8\ kg\ m^{-3}$ because *You and Tomczak* [1993] showed that the supply of ICW to the Northern Hemisphere occurs predominantly on the $\sigma_\theta = 26.7\ kg\ m^{-3}$ density surface, where isopycnal mixing predominates. Figure 8a shows that the T/S properties of waters within this density interval cluster around the linear ICW T/S properties, consistent with isopycnal mixing of ICW along the core density of $\sigma_\theta = 26.7\ kg\ m^{-3}$.

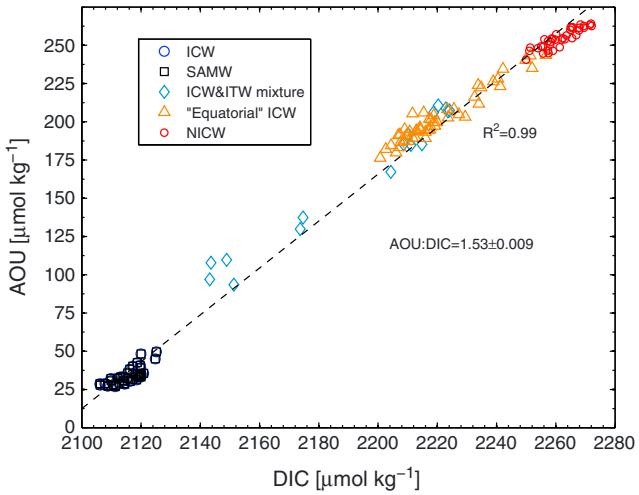

Figure 9. Scatterplot of DIC against AOU within the density intervals 26.6–26.8 kg m^{-3} from the southern reaches of the south Indian subtropical gyre (27°S) to the northernmost stations in the BoB (18°N). The AOU : DIC ratio is the slope (±1 SD) of the ordinary least squares fit shown as a dashed line.

As ICW is advected along the 26.7 kg m^{-3} density surface from the south Indian gyre to the BoB, where it has been renamed NICW (see section 3.3.1), it gradually loses oxygen and accumulates phosphate along its transport pathway. Thus, plotting phosphate against AOU from $\sigma_\theta = 26.6$ to 26.8 kg m^{-3} in NICW falls on the line of the phosphate versus AOU ordinary least squares regression obtained in ICW ($\sigma_\theta = 26.1$–26.8 kg m^{-3}) from the south Indian subtropical gyre (Figure 8b). In contrast, a scatterplot of nitrate and AOU for the ICW shows that the NICW falls below the ICW fit due to nitrate loss from denitrification processes in the oxygen-depleted waters of the Arabian Sea (Figure 8c). The nitrate and phosphate content of SAMW plot above the ICW regression line because SAMW forms in the subantarctic zone, where surface phosphate and nitrate levels are higher there than in the vicinity of the STF, where ICW is subducted (Figures 8b and 8c).

Since the regression of phosphate versus AOU in ICW allows predicting the phosphate content in the NICW end-member (Figure 8b), we can apply the same approach to dFe in order to determine if the subsurface dFe enrichment that we observed north of the SEC is sustained solely by remineralization of settling organic matter or if other sources may be supplying dFe. Figure 8d shows that the dFe in SAMW and the mixture of ICW/ITF waters cluster around the ICW fit. However, the data points from ICW in the equatorial domain (7.6°S–6.5°N) and from NICW in the BoB (>6.5°N) show significant scatter and plot above the dFe : AOU linear fit that characterizes ICW farther south in the gyre (Figure 8d). The decoupling between dFe and AOU in the northern Indian Ocean suggests that other dFe inputs, unrelated to *net* inputs of dFe via organic matter remineralization, supply additional dFe along the advective flow path of ICW. Possible sources of this extra dFe may result from (1) the interaction of ICW with sediments of the African shelf during its northward transit with the Somali Current or with sediments of the western coast of India and/or the southern tip of Sri Lanka as ICW is advected to the BoB via the West Indian Coast Current and SMC during the southwest monsoon; (2) the large input of dust impacting the surface waters of this region [*Grand et al.*, 2015], possibly combined with reduced scavenging losses in the oxygen depleted subsurface waters of the central and northern BoB (Figure 2b); and (3) sedimentary inputs from the deposition and resuspension of riverine sediments on the shelf in the northern BoB.

3.3.5. Fe : C Net Remineralization Ratios in Indian Central Water

In ICW of the south Indian subtropical gyre (27°S–16.3°S), where there is no evidence of hydrothermal or sedimentary inputs, the slope of the dFe : AOU relationship is 2.7 ± 0.8 µmol mol^{-1} ($n = 12$, $R^2 = 0.53$), and the intercept of the ordinary least squares regression implies a preformed dFe concentration of 0.14 ± 0.02 n*M* in the subduction region of ICW. This predicted preformed dFe concentration is comparable to the mean dFe (0.18 ± 0.05 n*M*, $n = 26$) observed from 48°S to 40°S where the $\sigma_\theta = 26.1$–26.6 kg m^{-3} isopycnals outcrop along the present section. It is also worth mentioning that the ICW dFe : AOU ratio in the gyre was remarkably similar to that observed in the ICW/ITW mixture farther north (2.9 ± 0.5 µmol mol^{-1}, $n = 19$, $R^2 = 0.67$), implying similar net remineralization rates of dFe in ICW and waters within the same density interval originating from the Indonesian Throughflow region.

Based on the slope of the ordinary least squares fit between DIC and AOU within the density intervals of ICW (Figure 9), we estimate that the oxidation of 1 mol of carbon consumes ~1.5 mol of oxygen during organic matter remineralization. Using our DIC : AOU and Fe : AOU ratios in ICW, we can calculate a net Fe : C remineralization ratio in ICW of 4.1 ± 1.5 µmol mol^{-1}. This ratio reflects the net release of dFe during organic

Table 2. Literature Compilation of Fe : C Remineralization Ratios in Various Ocean Basins[a]

Location	Water Mass	Fe : C × 10^{-6}	Reference
Indian Ocean subtropical gyre	ICW	4.1 ± 1.5	This work
North Atlantic	Not specified	9.9 ± 4.0	*Sunda* [1997]; *Johnson et al.* [1997]
North Atlantic subtropical gyre	NACW	6.6 ± 0.5	*Hatta et al.* [2014]
North Atlantic subtropical gyre	AEW	7.4 ± 1.0	*Hatta et al.* [2014]
Tropical North Atlantic	Not specified	11 ± 1.0	*Bergquist and Boyle* [2006]
Tropical North Atlantic	Not specified	9.6–12.4	*Fitzsimmons et al.* [2013]
North Pacific	Not specified	4.6 ± 2.7	*Sunda* [1997]; *Johnson et al.* [1997]
Equatorial Pacific	Not specified	2.0 ± 0.4	*Sunda* [1997]; *Johnson et al.* [1997]
Southern Ocean	Not specified	1.8 ± 0.4	*Sunda* [1997]; *Johnson et al.* [1997]

[a]All ratios were estimated using dFe and AOU in the water column. All Fe :C ratios are all in μmol mol^{-1} and show mean ± 1SD or reported range. Data from the *Sunda* [1997] reference are the mean Fe :C that was reported in each ocean basin of Table 1 in *Sunda* [1997].

matter remineralization along the flow path of ICW (i.e., dFe released during remineralization minus scavenging losses). Thus our Fe : C ratio is probably significantly lower than the elemental Fe : C stoichiometry of the original organic particles because a large proportion of the dFe released during organic matter remineralization will be lost via scavenging removal [*Twining and Baines,* 2013; *Hatta et al.*, 2014].

Our Fe : C ratio in ICW is significantly lower than that determined using similar approaches (i.e., calculated from regressions of dFe against AOU) in the North Atlantic Ocean (6.6–11 μmol mol^{-1}), comparable to Fe : C ratios from the North Pacific Ocean (~4.6 ± 2.7 μmol mol^{-1}) and higher than that calculated in the Equatorial Pacific and Southern Ocean (~1.8 ± 0.4 μmol mol^{-1}; Table 2). The magnitude of the Fe : C ratios from different oceanic regions is thought to scale with the degree of Fe availability in surface waters and the cellular Fe requirements of phytoplankton growing in each region [*Sunda*, 1997; *Twining and Baines*, 2013]. The geographical variations in Fe : C ratios may also scale with concentration of organic ligands in the subduction region of a water mass, since excess ligand levels may buffer dFe removal via inorganic scavenging in the ocean interior and hence produce elevated Fe : C ratios [*Tagliabue et al.,* 2014c]. Additional data along the advective pathway of water masses subjected to minimal diapycnal mixing and external dFe inputs in different oceanic regions will improve our understanding of the geochemical imprint of remineralization in the ocean interior.

4. Summary and Conclusions

The CLIVAR I08S and I09N sections cover a broad range of hydrographic and biogeochemical conditions and therefore reflect the effects of several source terms on the distributions of dFe and dAl in the eastern Indian Ocean. The distribution of dAl is mainly controlled by the large-scale gradients in dust deposition impacting the surface of the eastern Indian Ocean, the outflow of dissolved and suspended matter from the Ganges-Brahmaputra river system in the Bay of Bengal, and long-range subsurface transport of water masses labeled with dAl, particularly at the northern boundary of the Southern Ocean and possibly within the Indonesian Throughflow region.

In the Southern Ocean, the interaction of the ACC with the shallow topography of the southern Kerguelen Plateau appears to play a role in maintaining elevated subsurface dFe values that we observed below the mixed layer throughout the Antarctic Zone. We surmise that the strong offshore currents above the southern Kerguelen Plateau combined with enhanced vertical mixing rates could both contribute to the elevated subsurface dFe values observed there relative to other sectors of the Southern Ocean. Downstream of the northern Kerguelen Plateau, our dissolved and particulate dFe data may reflect long-range lateral inputs from the plateau's sediments, suggesting that shelf Fe inputs may be transported for up to ~1500 km away from the source region.

In the northern Indian Ocean, the South Equatorial Current (~15°S) marks a remarkable biogeochemical front separating the well-oxygenated and Fe-poor south Indian subtropical gyre waters from the oxygen-deficient and dFe-rich waters of the northern Indian Ocean and Bay of Bengal. Using the relationship between macronutrients, dFe and AOU in central waters occupying the south Indian subtropical gyre, we show that the subsurface waters of the northeast Indian Ocean and Bay of Bengal must receive extra dFe in addition to that produced during remineralization of settling organic matter. The resuspension of shelf sediments and release of pore waters along the pathway of Indian Central Water and in the Bay of Bengal probably contribute to the elevated Fe and Al levels observed there.

Acknowledgments
All data used in this paper are publicly available on the CLIVAR & Carbon Hydrographic Data Office website (CCHDO) using ExpoCodes 33RR20070204 and 33RR20070322 for I08S and I09N, respectively (http://cchdo.ucsd.edu). We thank the captain and crew of the R/V *Revelle*, chief scientists Jim Swift (I08S) and Janet Sprintall (I09N) and Kati Gosnell for their tremendous help and support during the seagoing part of this project. Thanks are due to Francois Ascani for his assistance with the preparation of Figure 4, Yoshiki Sohrin for sharing the data of the GEOTRACES-Japan expedition and to A. Tagliabue, and an anonymous reviewer for helpful comments. This work was funded by NSF OCE-0649584 to C.I.M., NSF-OCE-0649639 to W.M.L., and NSF OCE-61-4962 and 62–5889 to J.A.R. This is SOEST publication 9280, PMEL publication 4141, and JISAO publication 2223.

References

Alibo, D., and Y. Nozaki (2004), Dissolved rare earth elements in the eastern Indian Ocean: Chemical tracers of the water masses, *Deep Sea Res., Part I*, *51*, 559–576, doi:10.1016/j.dsr.2003.11.004.

Anderson, R., E. Mawji, G. Cutter, C. I. Measures, and C. Jeandel (2014), GEOTRACES: Changing the way we explore ocean chemistry, *Oceanography*, *27*(1), 50–61, doi:10.5670/oceanog.2014.07.

Archer, D., and K. Johnson (2000), A model of the iron cycle in the ocean, *Global Biogeochem. Cycles*, *14*(1), 269–279, doi:10.1029/1999GB900053.

Ardelan, M. V., C. D. Hewes, C. S. Reiss, N. S. Silva, H. Dulaiova, E. Steinnes, and E. Sakshaug (2010), Natural iron enrichment around the Antarctic Peninsula in the Southern Ocean, *Biogeosciences*, *7*, 11–25, doi:10.5194/bg-7-11-2010.

Aumont, O., E. Maier-Reimer, S. Blain, and P. Monfray (2003), An ecosystem model of the global ocean including Fe, Si, P colimitations, *Global Biogeochem. Cycles*, *17*(2), 1060, doi:10.1029/2001GB001745.

Barrett, P. M., J. A. Resing, N. J. Buck, C. S. Buck, W. M. Landing, and C. I. Measures (2012), The trace element composition of suspended particulate matter in the upper 1000 m of the eastern North Atlantic Ocean: A16N, *Mar. Chem.*, *142–144*, 41–53, doi:10.1016/j.marchem.2012.07.006.

Belkin, I., and A. Gordon (1996), Southern Ocean fronts from the Greenwich meridian to Tasmania, *J. Geophys. Res.*, *101*(C2), 3675–3696, doi:10.1029/95JC02750.

Bergquist, B. A., and E. A. Boyle (2006), Dissolved iron in the tropical and subtropical Atlantic Ocean, *Global Biogeochem. Cycles*, *20*, GB1015, doi:10.1029/2005GB002505.

Blain, S., G. Sarthou, and P. Laan (2008), Distribution of dissolved iron during the natural iron-fertilization experiment KEOPS (Kerguelen Plateau, Southern Ocean), *Deep Sea Res., Part II*, *55*(5–7), 594–605, doi:10.1016/j.dsr2.2007.12.028.

Bowie, A. R., D. Lannuzel, T. A. Remenyi, T. Wagener, P. J. Lam, P. W. Boyd, C. Guieu, A. T. Townsend, and T. W. Trull (2009), Biogeochemical iron budgets of the Southern Ocean south of Australia: Decoupling of iron and nutrient cycles in the subantarctic zone by the summertime supply, *Global Biogeochem. Cycles*, *23*, GB4034, doi:10.1029/2009GB003500.

Boyd, P. W., and M. J. Ellwood (2010), The biogeochemical cycle of iron in the ocean, *Nat. Geosci.*, *3*(10), 675–682, doi:10.1038/ngeo964.

Bucciarelli, E., S. Blain, and P. Tréguer (2001), Iron and manganese in the wake of the Kerguelen Islands (Southern Ocean), *Mar. Chem.*, *73*, 21–36, doi:10.1016/S0304-4203(00)00070-0.

Chever, F., G. Sarthou, E. Bucciarelli, S. Blain, and A. R. Bowie (2010), An iron budget during the natural iron fertilisation experiment KEOPS (Kerguelen Islands, Southern Ocean), *Biogeosciences*, *7*, 455–468, doi:10.5194/bg-7-455-2010.

Croot, P. L., K. Andersson, M. Öztürk, and D. R. Turner (2004), The distribution and speciation of iron along 6°E in the Southern Ocean, *Deep Sea Res., Part II*, *51*(22–24), 2857–2879, doi:10.1016/j.dsr2.2003.10.012.

de Baar, D., J. W. Hein, D. Jong, T. M. Jeroen, C. E. Dorothee, and M. Bettina (1995), Importance of iron for plankton blooms and carbon dioxide drawdown in the southern ocean, *Nature*, *373*, 412–415, doi:10.1038/373412a0.

De Jong, J., V. Schoemann, D. Lannuzel, P. Croot, H. de Baar, and J.-L. Tison (2012), Natural iron fertilization of the Atlantic sector of the Southern Ocean by continental shelf sources of the Antarctic Peninsula, *J. Geophys. Res.*, *117*, G01029, doi:10.1029/2011JG001679.

Dulaiova, H., M. V. Ardelan, P. B. Henderson, and M. A. Charette (2009), Shelf-derived iron inputs drive biological productivity in the southern Drake Passage, *Global Biogeochem. Cycles*, *23*, GB4014, doi:10.1029/2008GB003406.

Fine, R., W. Smethie, J. Bullister, M. Rhein, D.-H. Min, M. Warner, A. Poisson, and R. Weiss (2008), Decadal ventilation and mixing of Indian Ocean waters, *Deep Sea Res., Part I*, *55*, 20–37, doi:10.1016/j.dsr.2007.10.002.

Fine, R. A. (1993), Circulation of Antarctic intermediate water in the South Indian Ocean, *Deep Sea Res., Part I*, *40*(10), 2021–2042, doi:10.1016/0967-0637(93)90043-3.

Fitzsimmons, J. N., R. Zhang, and E. A. Boyle (2013), Dissolved iron in the tropical North Atlantic Ocean, *Mar. Chem.*, *154*, 87–99, doi:10.1016/j.marchem.2013.05.009.

Frew, R. D., D. A. Hutchins, S. Nodder, S. Sanudo-wilhelmy, A. Tovar-Sanchez, K. Leblanc, C. E. Hare, and P. W. Boyd (2006), Particulate iron dynamics during Fe cycle in subantarctic waters southeast of New Zealand, *Global Biogeochem. Cycles*, *20*, GB1S93, doi:10.1029/2005GB002558.

Gordon, A. L., S. Ma, D. B. Olson, P. Hacker, A. Ffield, L. D. Talley, D. Wilson, and M. Baringer (1997), Advection and diffusion of Indonesian Throughflow Water within the Indian Ocean South Equatorial Current, *Geophys. Res. Lett.*, *24*(21), 2573–2576, doi:10.1029/97GL01061.

Grand, M. M., C. S. Buck, W. M. Landing, C. I. Measures, M. Hatta, W. T. Hiscock, M. T. Brown, and J. A. Resing (2014), Quantifying the impact of atmospheric deposition on the biogeochemistry of Fe and Al in the upper ocean: A decade of collaboration with the US CLIVAR-CO_2 Repeat Hydrography Program, *Oceanography*, *27*(1), 62–65, doi:10.5670/oceanog.2014.08.

Grand, M. M., C. I. Measures, M. Hatta, W. T. Hiscock, C. S. Buck, and W. M. Landing (2015), Dust deposition in the eastern Indian Ocean: The ocean perspective from Antarctica to the Bay of Bengal, *Global Biogeochem. Cycles*, *29*, doi:10.1002/2014GB004898.

Hatta, M., C. I. Measures, K. Selph, M. Zhou, J. Yang, and W. T. Hiscock (2013), Iron fluxes from the shelf regions near the South Shetland Islands in the Drake Passage during the austral-winter 2006, *Deep Sea Res., Part II*, *90*, 89–101, doi:10.1016/j.dsr2.2012.11.003.

Hatta, M., C. I. Measures, J. Wu, S. Roshan, J. N. Fitzsimmons, P. Sedwick, and P. Morton (2014), An overview of dissolved Fe and Mn distributions during the 2010–2011 U.S. GEOTRACES North Atlantic cruises: GEOTRACES GA03, *Deep Sea Res., Part II*, doi:10.1016/j.dsr2.2014.07.005.

Hood, R., J. Wiggert, and S. Naqvi (2009), Indian Ocean research: Opportunities and challenges, in *Indian Ocean Biogeochemical Processes and Ecological Variability*, edited by J. Wiggert et al., pp. 409–428, AGU, Washington, D. C.

Hoppema, M., H. J. W. de Baar, E. Fahrbach, H. H. Hellmer, and B. Klein (2003), Substantial advective iron loss diminishes phytoplankton production in the Antarctic Zone, *Global Biogeochem. Cycles*, *17*(1), 1025, doi:10.1029/2002GB001957.

Jickells, T. D., et al. (2005), Global iron connections between desert dust, ocean biogeochemistry, and climate, *Science*, *308*(5718), 67–71, doi:10.1126/science.1105959.

Johnson, K. J., R. M. Gordon, and K. H. Coale (1997), What controls dissolved iron concentrations in the world ocean?, *Mar. Chem.*, *57*, 137–161, doi:10.1016/S0304-4203(97)00043-1.

Karstensen, J., and M. Tomczak (1997), Ventilation processes and water mass ages in the thermocline of the southeast Indian Ocean, *Geophys. Res. Lett.*, *24*(22), 2777–2780, doi:10.1029/97GL02708.

Klunder, M. B., P. Laan, R. Middag, H. J. W. De Baar, J. C. van Ooijen, and J. V. Ooijen (2011), Dissolved iron in the Southern Ocean (Atlantic sector), *Deep Sea Res., Part II*, *58*(25–26), 2678–2694, doi:10.1016/j.dsr2.2010.10.042.

Klunder, M. B., P. Laan, R. Middag, H. J. W. de Baar, and K. Bakker (2012), Dissolved iron in the Arctic Ocean: Important role of hydrothermal sources, shelf input and scavenging removal, *J. Geophys. Res.*, *117*, C04014, doi:10.1029/2011JC007135.

Klunder, M. B., P. Laan, H. J. W. De Baar, R. Middag, I. Neven, and J. Van Ooijen (2014), Dissolved Fe across the Weddell Sea and Drake Passage: Impact of DFe on nutrient uptake, *Biogeosciences*, *11*(3), 651–669, doi:10.5194/bg-11-651-2014.

Koch-Larrouy, A., R. Morrow, T. Penduff, and M. Juza (2010), Origin and mechanism of Subantarctic Mode Water formation and transformation in the Southern Indian Ocean, *Ocean Dyn.*, *60*(3), 563–583, doi:10.1007/s10236-010-0276-4.

Kondo, Y., and J. W. Moffett (2013), Dissolved Fe(II) in the Arabian Sea oxygen minimum zone and western tropical Indian Ocean during the inter-monsoon period, *Deep Sea Res., Part I*, *73*, 73–83, doi:10.1016/j.dsr.2012.11.014.

Koné, V., O. Aumont, M. Levy, and L. Resplandy (2009), Physical and biogeochemical controls of the phytoplankton seasonal cycle in the Indian Ocean: A modeling study, in *Indian Ocean Biogeochemical Processes and Ecological Variability*, edited by J. Wiggert et al., pp. 147–166, AGU, Washington, D. C.

Lannuzel, D., V. Schoemann, J. de Jong, J.-L. Tison, and L. Chou (2007), Distribution and biogeochemical behaviour of iron in the East Antarctic sea ice, *Mar. Chem.*, *106*(1–2), 18–32, doi:10.1016/j.marchem.2006.06.010.

Lannuzel, D., V. Schoemann, J. de Jong, B. Pasquer, P. van der Merwe, F. Masson, J.-L. Tison, and A. Bowie (2010), Distribution of dissolved iron in Antarctic sea ice: Spatial, seasonal, and inter-annual variability, *J. Geophys. Res.*, *115*, G03022, doi:10.1029/2009JG001031.

Lannuzel, D., P. C. van der Merwe, A. T. Townsend, and A. R. Bowie (2014), Size fractionation of iron, manganese and aluminium in Antarctic fast ice reveals a lithogenic origin and low iron solubility, *Mar. Chem.*, *161*, 47–56, doi:10.1016/j.marchem.2014.02.006.

Lin, H., S. Rauschenberg, C. R. Hexel, T. J. Shaw, and B. S. Twining (2011), Free-drifting icebergs as sources of iron to the Weddell Sea, *Deep Sea Res., Part II*, *58*(11–12), 1392–1406, doi:10.1016/j.dsr2.2010.11.020.

Martin, J. H. (1990), Glacial-interglacial CO_2 change: The iron hypothesis, *Paleoceanography*, *5*, 1–13, doi:10.1029/PA005i001p00001.

Martínez-Garcia, A., A. Rosell-Melé, W. Geibert, R. Gersonde, P. Masqué, V. Gaspari, and C. Barbante (2009), Links between iron supply, marine productivity, sea surface temperature, and CO_2 over the last 1.1 Ma, *Paleoceanography*, *24*, PA1207, doi:10.1029/2008PA001657.

Martínez-Garcia, A., D. M. Sigman, H. Ren, R. F. Anderson, M. Straub, D. A. Hodell, S. L. Jaccard, T. I. Eglinton, G. H. Haug, and A. Martínez-García (2014), Iron Fertilization of the Subantarctic Ocean During the Last Ice Age, *Science*, *343*(6177), 1347–1350, doi:10.1126/science.1246848.

McCartney, M. S., and K. A. Donohue (2007), A deep cyclonic gyre in the Australian-Antarctic Basin, *Prog. Oceanogr.*, *75*, 675–750, doi:10.1016/j.pocean.2007.02.008.

Measures, C. I., and E. Brown (1996), Estimating dust input to the Atlantic Ocean using surface water aluminium concentrations, in *The Impact of Desert Dust Across the Mediterranean*, edited by S. Guerzoni and R. Chester, pp. 301–311, Kluwer Acad., Netherlands.

Measures, C. I., and S. Vink (1999), Seasonal variations in the distribution of Fe and Al in the surface waters of the Arabian Sea, *Deep Sea Res., Part II*, *46*, 1597–1622, doi:10.1016/S0967-0645(99)00037-5.

Measures, C. I., and S. Vink (2000), On the use of dissolved aluminium in surface waters to estimate dust deposition to the ocean, *Global Biogeochem. Cycles*, *14*(1), 317–327, doi:10.1029/1999GB001188.

Measures, C. I., and S. Vink (2001), Dissolved Fe in the upper waters of the Pacific sector of the Southern Ocean, *Deep Sea Res., Part II*, *48*(19–20), 3913–3941, doi:10.1016/S0967-0645(01)00074-1.

Measures, C. I., J. Yuan, and J. A. Resing (1995), Determination of iron in seawater by flow injection analysis using in-line preconcentration and spectrophotometric detection, *Mar. Chem.*, *50*, 1–10.

Measures, C. I., W. M. Landing, M. T. Brown, and C. S. Buck (2008a), High-resolution Al and Fe data from the Atlantic Ocean CLIVAR-CO_2 Repeat Hydrography A16N transect: Extensive linkages between atmospheric dust and upper ocean geochemistry, *Global Biogeochem. Cycles*, *22*, GB1005, doi:10.1029/2007GB003042.

Measures, C. I., W. M. Landing, M. T. Brown, and C. S. Buck (2008b), A commercially available rosette system for trace metal clean sampling, *Limnol. Oceanogr. Methods*, *6*, 384–394, doi:10.4319/lom.2008.6.384.

Measures, C. I., M. T. Brown, K. E. Selph, A. Apprill, M. Zhou, M. Hatta, and W. T. Hiscock (2013), The influence of shelf processes in delivering dissolved iron to the HNLC waters of the Drake Passage, Antarctica, *Deep Sea Res., Part II*, *90*, 77–88, doi:10.1016/j.dsr2.2012.11.004.

Middag, R., H. de Baar, P. Laan, and K. Bakker (2009), Dissolved aluminium and the silicon cycle in the Arctic Ocean, *Mar. Chem.*, *115*, 176–195, doi:10.1016/j.marchem.2009.08.002.

Middag, R., C. van Slooten, H. J. W. de Baar, and P. Laan (2011), Dissolved aluminium in the Southern Ocean, *Deep Sea Res., Part II*, *58*(25–26), 2647–2660, doi:10.1016/j.dsr2.2011.03.001.

Middag, R., H. J. W. de Baar, P. Laan, and O. Huhn (2012), The effects of continental margins and water mass circulation on the distribution of dissolved aluminum and manganese in Drake Passage, *J. Geophys. Res.*, *117*, C01019, doi:10.1029/2011JC007434.

Middag, R., H. J. W. de Baar, M. B. Klunder, and P. Laan (2013), Fluxes of dissolved aluminum and manganese to the Weddell Sea and indications for manganese co-limitation, *Limnol. Oceanogr.*, *58*(1), 287–300, doi:10.4319/lo.2013.58.1.0287.

Milliman, J., and R. Meade (1983), World-wide delivery of river sediment to the oceans, *J. Geol.*, *91*, 1–21, doi:10.1086/628741.

Misumi, K., K. Lindsay, J. K. Moore, S. C. Doney, D. Tsumune, and Y. Yoshida (2013), Humic substances may control dissolved iron distributions in the global ocean: Implications from numerical simulations, *Global Biogeochem. Cycles*, *27*, 450–462, doi:10.1002/gbc.20039.

Moffett, J. W., T. J. Goepfert, and S. W. A. Naqvi (2007), Reduced iron associated with secondary nitrite maxima in the Arabian Sea, *Deep Sea Res., Part I*, *54*(8), 1341–1349, doi:10.1016/j.dsr.2007.04.004.

Mongin, M. M., E. R. Abraham, and T. W. Trull (2009), Winter advection of iron can explain the summer phytoplankton bloom that extends 1000 km downstream of the Kerguelen Plateau in the Southern Ocean, *J. Mar. Res.*, *67*(2), 225–237, doi:10.1357/002224009789051218.

Moore, J. K., and M. R. Abbott (2000), Phytoplankton chlorophyll distributions and primary production in the Southern Ocean, *J. Geophys. Res.*, *105*(C12), 28,709–28,722, doi:10.1029/1999JC000043.

Moore, J. K., and O. Braucher (2008), Sedimentary and mineral dust sources of dissolved iron to the world ocean, *Biogeosciences*, *5*, 631–656, doi:10.5194/bg-5-631-2008.

Nath, B. N., V. P. Rao, and K. P. Becker (1989), Geochemical evidence of terrigenous influence in deep-sea sediments up to 8°S in the Central Indian Basin, *Mar. Geol.*, *87*(2–4), 301–313, doi:10.1016/0025-3227(89)90067-4.

Nishioka, J., T. Ono, H. Saito, K. Sakaoka, and T. Yoshimura (2011), Oceanic iron supply mechanisms which support the spring diatom bloom in the Oyashio region, western subarctic Pacific, *J. Geophys. Res.*, *116*, C02021, doi:10.1029/2010JC006321.

Nishioka, J., H. Obata, and D. Tsumune (2013), Evidence of an extensive spread of hydrothermal dissolved iron in the Indian Ocean, *Earth Planet. Sci. Lett.*, *361*, 26–33, doi:10.1016/j.epsl.2012.11.040.

Nozaki, Y., and D. S. Alibo (2003), Importance of vertical geochemical processes in controlling the oceanic profiles of dissolved rare earth elements in the northeastern Indian Ocean, *Earth Planet. Sci. Lett.*, *205*, 155–172, doi:10.1016/S0012-821X(02)01027-0.

Nozaki, Y., and Y. Yamamoto (2001), Radium 228 based nitrate fluxes in the eastern Indian Ocean and the South China Sea and a silicon-induced "alkalinity pump" hypothesis, *Global Biogeochem. Cycles*, *15*(3), 555–567, doi:10.1029/2008GB003406.

Obata, H., Y. Nozaki, D. S. Alibo, and Y. Yamamoto (2004), Dissolved Al, In, and Ce in the eastern Indian Ocean and the Southeast Asian Seas in comparison with the radionuclides 210 Pb and 210 Po, *Geochim. Cosmochim. Acta*, *68*(5), 1035–1048, doi:10.1016/j.gca.2003.07.021.

Orsi, A. H., T. I. I. I. Whitworth, and W. D. J. Nowlin (1995), On the meridional extent and fronts of the Antarctic Circumpolar Current, *Deep Sea Res., Part I*, *42*, 641–673, doi:10.1016/0967-0637(95)00021-W.

Parekh, P., M. J. Follows, and E. A. Boyle (2004), Modeling the global ocean iron cycle, *Global Biogeochem. Cycles*, *18*, GB1002, doi:10.1029/2003GB002061.

Parekh, P., M. J. Follows, and E. A. Boyle (2005), Decoupling of iron and phosphate in the global ocean, *Global Biogeochem. Cycles*, *19*, GB2020, doi:10.1029/2004GB002280.
Park, Y. H., E. Charriaud, and M. Fieux (1998), Thermohaline structure of the Antarctic Surface Water/Winter Water in the Indian sector of the Southern Ocean, *J. Mar. Syst.*, *17*(1–4), 5–23, doi:10.1016/S0924-7963(98)00026-8.
Park, Y.-H., J. Fuda, I. Durand, and A. Naveiragarabato (2008), Internal tides and vertical mixing over the Kerguelen Plateau, *Deep Sea Res., Part II*, *55*(5–7), 582–593, doi:10.1016/j.dsr2.2007.12.027.
Park, Y.-H., F. Vivier, F. Roquet, and E. Kestenare (2009), Direct observations of the ACC transport across the Kerguelen Plateau, *Geophys. Res. Lett.*, *36*, L18603, doi:10.1029/2009GL039617.
Planquette, H., et al. (2007), Dissolved iron in the vicinity of the Crozet Islands, Southern Ocean, *Deep Sea Res., Part II*, *54*(18–20), 1999–2019, doi:10.1016/j.dsr2.2007.06.019.
Prasanna Kumar, S., P. Muraleedharan, T. Prasad, M. Gauns, N. Ramaiah, S. de Souza, S. Sardesai, and M. Madhupratap (2002), Why is the Bay of Bengal less productive during summer monsoon compared to the Arabian Sea?, *Geophys. Res. Lett.*, *29*(24), 2235, doi:10.1029/2002GL016013.
Reid, J. L. (2003), On the total geostrophic circulation of the Indian Ocean: Flow patterns, tracers, and transports, *Prog. Oceanogr.*, *56*, 137–186, doi:10.1016/S0079-6611(02)00141-6.
Resing, J. A., and C. I. Measures (1994), Fluorometric determination of Al in seawater by flow injection analysis with in-line preconcentration, *Anal. Chem.*, *66*, 4105–4111.
Rijkenberg, M. J. A., R. Middag, P. Laan, L. J. A. Gerringa, H. M. van Aken, V. Schoemann, J. T. M. de Jong, and H. J. W. de Baar (2014), The distribution of dissolved iron in the west Atlantic Ocean, *PLoS One*, *9*(6), e101323, doi:10.1371/journal.pone.0101323.
Rintoul, S. R., S. Sokolov, and R. A. Massom (2008), Rapid development and persistence of a massive Antarctic sea ice tongue, *J. Geophys. Res.*, *113*, C07045, doi:10.1029/2007JC004541.
Roquet, F., Y.-H. Park, C. Guinet, F. Bailleul, and J.-B. Charrassin (2009), Observations of the Fawn Trough Current over the Kerguelen Plateau from instrumented elephant seals, *J. Mar. Syst.*, *78*(3), 377–393, doi:10.1016/j.jmarsys.2008.11.017.
Saager, P. M., H. J. W. De Baar, and P. H. Burkill (1989), Manganese and iron in Indian Ocean waters, *Geochim. Cosmochim. Acta*, *53*(9), 2259–2267, doi:10.1016/0016-7037(89)90348-7.
Sarthou, G., C. Jeandel, L. Brisset, D. Amouroux, T. Besson, and O. Donard (1997), Fe and H_2O_2, distributions in the upper water column in the Indian sector of the Southern Ocean, *Earth Planet. Sci. Lett.*, *147*, 83–92.
Schlitzer, R. (2014), Ocean data view. [Available at http://odv.awi.]
Schott, F. A., and J. P. McCreary (2001), The monsoon circulation of the Indian Ocean, *Prog. Oceanogr.*, *51*(1), 1–123, doi:10.1016/S0079-6611(01)00083-0.
SCOR Working Group (2007), GEOTRACES – An international study of the global marine biogeochemical cycles of trace elements and their isotopes, *Chem. Erde*, *67*, 85–131, doi:10.1016/j.chemer.2007.02.001.
Sedwick, N., R. Bowie, and W. Trull (2008), Dissolved iron in the Australian sector of the Southern Ocean (CLIVAR SR3 Section): Meridional and seasonal trends, *Deep Sea Res., Part I*, *55*, 911–925, doi:10.1016/j.dsr.2008.03.011.
Siedler, G., M. Rouault, and J. R. E. Lutjeharms (2006), Structure and origin of the subtropical South Indian Ocean Countercurrent, *Geophys. Res. Lett.*, *33*, L24609, doi:10.1029/2006GL027399.
Singh, S. P., S. K. Singh, V. Goswami, R. Bhushan, and V. K. Rai (2012), Spatial distribution of dissolved neodymium and εNd in the Bay of Bengal: Role of particulate matter and mixing of water masses, *Geochim. Cosmochim. Acta*, *94*, 38–56, doi:10.1016/j.gca.2012.07.017.
Sohrin, Y., S. Iwamoto, M. Matsui, H. Obata, E. Nakayama, K. Suzuki, N. Handa, and M. Ishii (2000), The distribution of Fe in the Australian sector of the Southern Ocean, *Deep Sea Res., Part I*, *47*, 55–84, doi:10.1016/S0967-0637(99)00049-7.
Sokolov, S., and S. R. Rintoul (2007), On the relationship between fronts of the Antarctic Circumpolar Current and surface chlorophyll concentrations in the Southern Ocean, *J. Geophys. Res.*, *112*, C07030, doi:10.1029/2006JC004072.
Subramanian, V., L. Van't Dack, and R. Van Grieken (1985), Chemical composition of river sediments from the Indian sub-continent, *Chem. Geol.*, *48*, 271–179, doi:10.1016/0009-2541(85)90052-X.
Sunda, W. G. (1997), Control of dissolved iron concentrations in the world ocean, a comment, *Mar. Chem.*, *57*(3–4), 169–172, doi:10.1016/S0304-4203(97)00045-5.
Tagliabue, A., T. Mtshali, O. Aumont, A. R. Bowie, M. B. Klunder, A. N. Roychoudhury, and S. Swart (2012), A global compilation of dissolved iron measurements: Focus on distributions and processes in the Southern Ocean, *Biogeosciences*, *9*(6), 2333–2349, doi:10.5194/bg-9-2333-2012.
Tagliabue, A., O. Aumont, and L. Bopp (2014a), The impact of different external sources of iron on the global carbon cycle, *Geophys. Res. Lett.*, *41*, 920–926, doi:10.1002/2013GL059059.
Tagliabue, A., J.-B. Sallée, A. R. Bowie, M. Lévy, S. Swart, and P. W. Boyd (2014b), Surface-water iron supplies in the Southern Ocean sustained by deep winter mixing, *Nat. Geosci.*, *7*(4), 314–320, doi:10.1038/ngeo2101.
Tagliabue, A., R. G. Williams, N. Rogan, E. P. Achterberg, and P. W. Boyd (2014c), A ventilation-based framework to explain the regeneration-scavenging balance of iron in the ocean, *Geophys. Res. Lett.*, *41*, 1–10, doi:10.1002/2014GL061066.
Takao, S., T. Hirawake, S. W. Wright, and K. Suzuki (2012), Variations of net primary productivity and phytoplankton community composition in the Indian sector of the Southern Ocean as estimated from ocean color remote sensing data, *Biogeosciences*, *9*(10), 3875–3890, doi:10.5194/bg-9-3875-2012.
Talley, L. D., and J. Sprintall (2005), Deep expression of the Indonesian Throughflow: Indonesian Intermediate Water in the South Equatorial Current, *J. Geophys. Res.*, *110*, C10009, doi:10.1029/2004JC002826.
Talley, L. D., G. L. Pickard, W. J. Emery, and J. H. Swift (2011), *Descriptive Physical Oceanography: An Introduction*, 6th ed., Elsevier Inc., Oxford, U. K.
Tomczak, M., and J. Godfrey (2003), *Regional Oceanography: An Introduction*, 2nd ed., Daya House, Delhi.
Twining, B. S., and S. B. Baines (2013), The trace metal composition of marine phytoplankton, *Annu. Rev. Mar. Sci.*, *5*, 191–215, doi:10.1146/annurev-marine-121211-172322.
Unger, D., V. Ittekkot, P. Schäfer, J. Tiemann, and S. Reschke (2003), Seasonality and interannual variability of particle fluxes to the deep Bay of Bengal: Influence of riverine input and oceanographic processes, *Deep Sea Res., Part II*, *50*(5), 897–923, doi:10.1016/S0967-0645(02)00612-4.
van Beusekom, J. E. E., A. J. V. Van Bennekom, J. Morvans, P. Treguer, and J. Morvan (1997), Aluminium and silicic acid in water and sediments of the Enderby and Crozet Basins, *Deep Sea Res., Part II*, *44*(5), 987–1003, doi:10.1016/S0967-0645(96)00105-1.
Van Hulten, M. M. P., A. Sterl, R. Middag, H. J. W. de Baar, M. Gehlen, J.-C. Dutay, and A. Tagliabue (2014), On the effects of circulation, sediment resuspension and biological incorporation by diatoms in an ocean model of aluminium*, *Biogeosciences*, *11*(14), 3757–3779, doi:10.5194/bg-11-3757-2014.
Vinayachandran, P., and T. Yamagata (1998), Monsoon response of the sea around Sri Lanka: Generation of thermal domes and anticyclonic vortices, *J. Phys. Oceanogr.*, *28*, 1946–1960.

Vinayachandran, P. N., P. Chauhan, M. Mohan, and S. Nayak (2004), Biological response of the sea around Sri Lanka to summer monsoon, *Geophys. Res. Lett.*, *31*, L01302, doi:10.1029/2003GL018533.

Vu, H. T. D., and Y. Sohrin (2013), Diverse stoichiometry of dissolved trace metals in the Indian Ocean, *Sci. Rep.*, *3*, 1745, doi:10.1038/srep01745.

Whitworth, T., and W. D. Nowlin (1987), Water masses and currents of the Southern Ocean at the Greenwich Meridian, *J. Geophys. Res.*, *92*(C6), 6462–6476, doi:10.1029/JC092iC06p06462.

Wong, A. P. S. (2005), Subantarctic Mode Water and Antarctic Intermediate Water in the South Indian Ocean based on profiling float data 2000–2004, *J. Mar. Res.*, *63*(4), 789–812, doi:10.1357/0022240054663196.

You, Y. (1997), Seasonal variations of thermocline circulation and ventilation in the Indian Ocean, *J. Geophys. Res.*, *102*(C5), 10,391–10,422, doi:10.1029/96JC03600.

You, Y., and M. Tomczak (1993), Thermocline circulation and ventilation in the Indian Ocean derived from water mass analysis, *Deep Sea Res., Part I*, *40*(1), 13–56, doi:10.1016/0967-0637(93)90052-5.